MULLARD LIMITED
Mullard House
Torrington Place
London, W.C.1

CONTENTS

Germanium Microwave Diodes for Broadband Mixer and Low Level Detector Applications 122-132

Advanced Techniques in Radio Frequency Heating Generator Design 133-134

Dielectric Heater Using Half-wave Line at 30MHz 135-145

A 400kHz Induction Heater of Advanced Design for Powers up to 60kW 146-149

A 300kHz Induction Heater of Advanced Design for Powers up to 120kW/240kW 150-156

VOL. 10 No. 94 JULY 1968

Mullard Technical Communications

VOLUME 10 NUMBER 94

July 1968

Mullard Technical Communications

VOLUME 10 NUMBER 94 July 1968

Contents

Germanium Microwave Diodes for Broadband Mixer and Low Level Detector Applications *T. H. Oxley* 122

Advanced Techniques in Radio Frequency Heating Generator Design *H. F. Dittrich* 133

Dielectric Heater Using Half-wave Line at 30MHz *H. F. Dittrich* 135

A 400kHz Induction Heater of Advanced Design for Powers up to 60kW *D. E. Nightingale* 146

A 300kHz Induction Heater of Advanced Design for Powers up to 120kW/240kW *D. E. Nightingale* 150

Mullard Technical Communications contains information on the performance or application of Mullard products such as semiconductor devices, integrated circuits, electronic valves and tubes, and electrical and magnetic components. It is issued free-of-charge to equipment designers, research organisations, reference libraries, and educational establishments. Applications to be added to the circulation list should be made under an official letter head to Central Technical Services.

Abstracts, or references to an article, should mention both the source, *Mullard Technical Communications*, and the authors. Requests for republication or translation should be made to the Editor in writing.

All articles in *Mullard Technical Communications* are indexed in *British Technology Index*. Abstracts appear in *Current Papers in Physics, Electrotechnology, and Control*.

The issue of the information contained in this publication does not imply any authority or licence for the utilisation of any patented feature.

'Mullard' is the trade mark of Mullard Limited and is registered in most of the principal countries of the world.

Editor: F. A. Sowan
Assistant Editors: E. G. Evans A. Perry

Published by
Central Technical Services
Mullard Limited, Mullard House, Torrington Place, London, W.C.1
Telephone: 01-580 6633 Telex: 264341

© Mullard Limited, 1968

Made and Printed in England by
WIGHTMAN AND COMPANY LIMITED, 1/3 BRIXTON ROAD, LONDON, S.W.9

Germanium Microwave Diodes for Broadband Mixer and Low Level Detector Applications

T. H. Oxley
Associated Semiconductor Manufacturers Limited, Wembley Laboratories

This article discusses the performance of advanced conventional germanium point contact diodes designed specifically for broadband low noise mixer applications, and bonded backward diodes intended for broadband high sensitivity low level detector applications.

The fabrication of these devices in a novel miniature double ended encapsulation ensures: wide frequency application, wide bandwidth properties, extremely rugged reversible construction, and adaptability to standard coaxial outlines.

The results indicate that superheterodyne receiver noise figures as low as 5·5dB, 6·0dB and 7·0dB may be achieved at S-band, X-band and J(Ku)-band frequencies respectively with use of the conventional mixer diode, whilst the bonded backward detector achieves a tangential sensitivity performance of about −54dbm for frequencies up to 18GHz.

Finally, the resistance of these devices to damage by electrical overloads and their r.f. performance as a function of temperature are considered.

INTRODUCTION

This article describes some recent advances in the performance of microwave diodes applied as frequency changers and low level detectors specifically designed for broadband applications. Devices primarily considered are the conventional metal-semiconductor germanium point contact diode and the bonded backward diode.

The conventional point contact and more recently introduced Schottky barrier diodes are metal-semiconductor devices which are described by the Schottky theory of rectification at a metal-semiconductor junction. The main difference between the two is their construction; the junction of the point contact device is formed with a metal wire in pressure contact with the semiconductor surface, whilst the junction of the Schottky barrier device is formed with an evaporated contact. The merits of the two technological approaches together with the merits of the semiconductor material for these devices have been described in previous literature (Refs. 1, 2). Briefly, it has been shown theoretically that, due to their mobilities, gallium arsenide may be expected to achieve the highest cut-off frequency, followed by germanium and then silicon, for either technology. However, for frequencies up to about X-band it has been shown that the merits of gallium arsenide and germanium are comparable for point contact technology, and further, comparable ideal conversion loss performance is achieved with either technology. Obvious advantages of the Schottky barrier techniques are maintenance of the required clean interface between metal and semiconductor, elimination of possible instability of a whisker pressure contact, and compatibility with integration. However, it is difficult to fabricate Schottky barrier devices with junction capacitances as small as with point contact techniques, and at present for encapsulated devices this is the prime technical advantage of point contact technology.

The tunnel diode or Esaki diode is a p–n junction diode exhibiting quantum mechanical tunnelling. The diode itself is made of heavily doped semiconductor material and is an abrupt junction with an extremely narrow depletion layer. Much of the importance of the tunnel diode arises from its negative resistance characteristic, but in the case of the backward diode the tunnelling is reduced from the high levels of a conventional tunnel diode to such levels that a negative resistance is almost non-existent. The tunnel diode, although capable of microwave mixing and detecting, is difficult to stabilise, and the negative conductance is a circuit problem. A good compromise is a backward diode, and its type of characteristic is normally used for microwave mixer and detector applications. Carrier concentrations of about $10^{19}/\text{cm}^3$ are required, and a high mobility is desired to minimise spreading resistance. Germanium, gallium antimonide and gallium arsenide all have acceptable properties. At present, however, microwave diodes are normally fabricated from n-type germanium with a gallium or aluminium doped junction, and alloyed junction and pulse-bonded techniques are the chief methods at present employed for their fabrication. The pulse bonded structure (with its associated small contact area and low capacitance) is an attractive method to obtain the required capacitance for microwave frequencies (Ref. 3) and has the advantage of control of r.f. impedance.

DIODE RECTIFIER CHARACTERISTICS

The basic microwave frequency characteristics of a diode rectifier are its input r.f. admittance and sensitivity; sensitivity being expressed either in terms of receiver overall noise figure for mixer applications or figure of merit for detector applications.

Point contact and backward diodes may be described electrically by the simple equivalent circuit shown in Fig. 1, where C_B is the barrier capacitance, R_B is the barrier resistance and R_S is the series resistance. The encapsulation parameters are represented by the series inductance L_S and the case capacitance C.

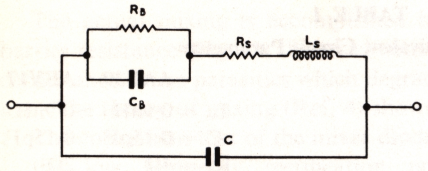

Fig. 1—Simple diode equivalent circuit

For a mixer diode which normally operates under large signal conditions (that is, with local oscillator powers of about a milliwatt), the rectification efficiency is the ratio of conductance in the forward direction to the admittance in the reverse direction and may be given (Ref. 4) by:

$$\eta = 1 - j\frac{1}{\omega C_B R_S}. \qquad \ldots(1)$$

For a detector diode, signal levels are normally low (that is, in the microwatt region) and the concept of front/back ratio for the mixer applications has little significance. The equivalent circuit becomes a current generator shunted by the barrier admittance, and the diode operates as a square law device. The diode sensitivity is determined by the microwave short circuit current sensitivity and may be given (Ref. 4) by the relation:

$$\beta = \frac{\beta_o}{1+\omega^2 C_B{}^2 R_B R_S} \qquad \ldots(2)$$

where β_o is the low frequency current sensitivity determined by the curvature of the I–V characteristic at the operating point.

Thus for high efficiency, C_B and R_S must be minimised for mixer and detector considerations, with detector sensitivity depending on the square of C_B in contrast to linear dependence for the mixer.

From the equivalent circuit of Fig. 1, the r.f. admittance of the diode rectifier may be given by:

$$\frac{1}{Z} = \frac{1}{\dfrac{1}{(1/R_B)+j\omega C_B} + j\omega L_S + R_S} + j\omega C. \qquad \ldots(3)$$

Obviously the equivalent circuit has two resonant frequencies, the series and the parallel, in the neighbourhood of which a considerable change in r.f. admittance will occur. If the ohmic resistances R_B and R_S are neglected, then in the case of the series resonance, the admittance of the tuned circuit is infinity and the resonant frequency is:

$$\omega_{\text{series res}} = \frac{1}{(L_S C_B)^{\frac{1}{2}}}. \qquad \ldots(4)$$

In the case of the parallel resonance, the admittance of the tuned circuit is zero and the resonant frequency is:

$$\omega_{\text{parallel res}} = \omega_{\text{series res}}[1+(C_B/C)]^{\frac{1}{2}}. \qquad \ldots(5)$$

Thus the values of the frequencies corresponding to the series and parallel resonance are determined by the values of L_S, C_B and C. By adjusting the values of these parameters it is possible to adjust the resonant frequencies of the diode rectifier, and hence the device r.f. admittance for a given design frequency.

In practice, the case capacitance is usually about 0·2pF, and small variations encountered do not significantly affect the frequency characteristics of the device. For broadband properties, therefore, the parameters C_B and L_S have the most significance and it is obviously desirable to minimise these values. Reduction of the barrier capacitance C_B is consistent with the requirements for device efficiency, thus minimising this parameter is of prime importance for broadband high efficiency device operation.

ENCAPSULATION

Types of encapsulation in current use are shown in Fig. 2. The cartridge and large coaxial types are suitable for use at frequencies up to about 12GHz, the small coaxial type for frequencies up to 18GHz, the plug-in waveguide for the frequency range 26 to 40GHz and the recently introduced miniature double ended capsule for frequencies up to at least 40GHz. In fact this last type of encapsulation has been used successfully as high as 140GHz (Ref. 1).

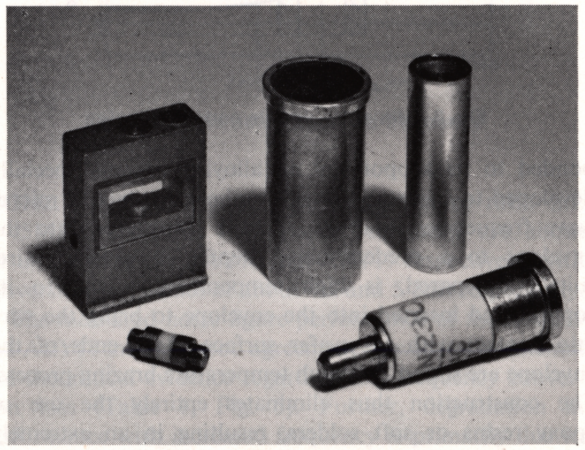

Fig. 2—Microwave diode encapsulations

The X-band cartridge of the 1N23 type is designed primarily for use across full height X-band waveguide, and the high r.f. impedance necessary to match the characteristic impedance of the waveguide is achieved chiefly by a large series inductance (about 5nH), resulting in a series resonant frequency of about 6GHz; whereas the relatively smaller series inductance (about 1nH) of the miniature double ended capsule increases the series resonant frequency for a similar barrier capacitance to about 12GHz.

The high resonant frequency and small configuration of the miniature double ended capsule suggest potential broadband properties and versatility. Not only is it suitable for an extremely wide frequency range, but it is also suitable for waveguide, coaxial and stripline applications and is of course reversible. Further, its configuration suggests it is possible to adapt it to standard outlines. This aspect is discussed on page 129.

The cross-section of the miniature double ended capsule assembly in Fig. 3 shows the method of construction. The end caps are formed from titanium and are bonded to the centre high alumina ceramic insulating tube by an active alloying brazing process, to form the metal ceramic envelope. The whisker and semiconductor wafer supports are made from a low thermal expansion material (to match that of titanium) and are inserted into the envelope. The semiconductor wafer is suitably prepared and is then

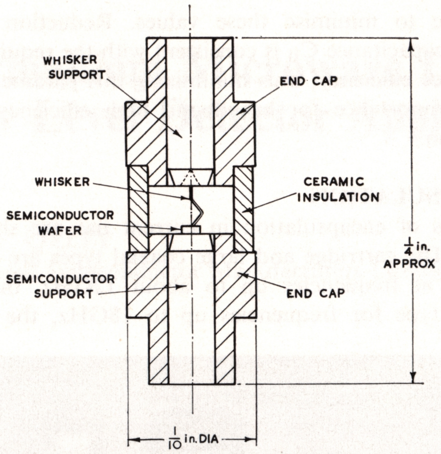

Fig. 3—Miniature double ended capsule

bonded to its support by an alloying process specially developed to ensure a low noise ohmic contact at microwave frequencies, and the support is inserted into the envelope to a predetermined depth. A whisker wire, suitably prepared, is high temperature brazed to its support and inserted into the envelope to bring the wire into contact with the wafer surface. Both ends of the envelope are sealed by a high temperature brazing process. The construction thus eliminates entirely the use of epoxy resins or soft solders, resulting in an extremely robust and hermetically sealed reversible capsule, capable of withstanding a wide temperature range.

In the case of the germanium point contact device, the whisker is prepared from titanium and the semiconductor wafer from n-type germanium; the metal-semiconductor rectifying contact is electro-formed by capacitance discharge techniques to form the desired electrical diode characteristics. The bonded backward diode employs a gallium-plated gold whisker wire, the junction being formed on low resistivity n-type germanium with pulse bonding techniques to alloy the tip of the whisker to the semiconductor wafer.

DEVICES FABRICATED IN MINIATURE DOUBLE ENDED CAPSULE

The Mullard types AAY34, AAY39 and AEY17 are examples of devices fabricated in the miniature double ended capsule. The AAY34 and AAY39 are conventional germanium point contact diodes primarily designed for low noise mixer applications. The AEY17 is a bonded backward diode primarily designed for high sensitivity broadband detector applications. The AAY34 was designed originally for Q(Ka)-band frequencies, and the AAY39 followed a logical development from that type, but with advanced technology resulting in enhanced performance.

The remainder of this article describes the electrical performance of the AAY39 and AEY17, with special attention, where possible, to comparison of their characteristics, thus illustrating the merits of conventional germanium point contact and bonded backward devices for particular applications.

A brief study of their low frequency and equivalent circuit parameters is a useful introduction to these devices.

TABLE 1

Typical Equivalent Circuit Parameters

		AAY39	AEY17
Case series inductance	$L_s =$	0·9nH	0·9nH
Case capacitance	$C =$	0·15pF	0·15pF
Diode series resistance	$R_s =$	4Ω	2Ω
Diode barrier resistance	$R_B =$	250Ω	300Ω
Diode barrier capacitance	$C_B =$	0·2pF	0·3pF
Forward I–V characteristic exponent	$n =$	9	2
Low frequency conversion loss (Image matched)	$L_c =$	3·7dB	5·5dB

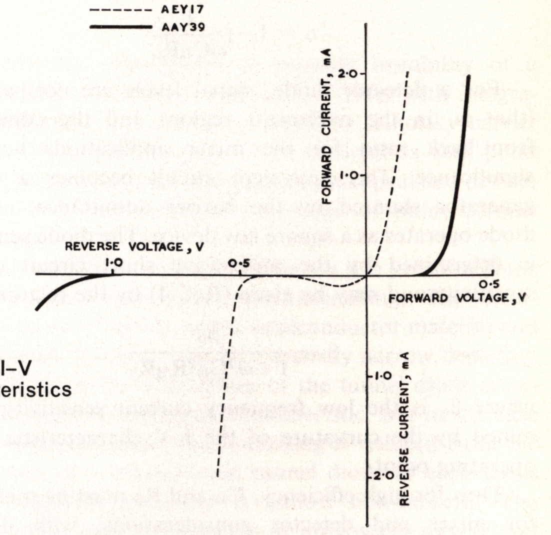

Fig. 4—I–V characteristics

These are summarised in Table 1, with their I–V characteristics illustrated in Fig. 4.

MIXER APPLICATIONS

A convenient way of expressing the performance of a microwave mixer diode is in terms of the overall noise figure F_o of a superheterodyne receiver.

It may be shown (Ref. 4) that

$$F_o = L_C(F_{i.f.} + N_r - 1) \qquad \ldots(6)$$

assuming any local oscillator noise is suppressed, where L_C is the conversion loss of the mixer diode, N_r is the noise temperature ratio of the mixer diode, and $F_{i.f.}$ is the noise figure of the following i.f. amplifier.

The double channel or image matched input circuit is favoured for most microwave receiver applications, and the noise figure performance of mixer diodes is measured and specified under these conditions (normally termed the broadband case; that is, when the same load admittance is presented to the image and signal channels). The theoretical limit for the diode conversion loss set by this condition is 3dB, thus the theoretical limit for the receiver performance (assuming $N_r = 1$) is given by:

$$F_o = 2F_{i.f.} \qquad \ldots(7)$$

for example, 4·5dB for an i.f. amplifier with a noise figure of 1·5dB.

Eq. 6 shows that the conversion loss L_C and the noise temperature ratio N_r are the mixer diode parameters determining the performance of the receiver, and these should be minimised.

The actual mixing is accomplished by the non-linear barrier resistance (Fig. 1); the series resistance and barrier capacitance act as parasitics which degrade the conversion loss. The theory of mixing (Ref. 4) shows that:

1) The conversion loss of the mixer diode is dependent on the low frequency rectification properties of the junction, and if R_B is large under conditions of reverse bias, this is primarily a function of the forward I–V characteristic exponent n (Ref. 5) where n is the slope of the log current versus log voltage curve of the diode I–V characteristic.
2) At any frequency at which the barrier capacitance is significant, the product C_BR_S must be minimised for optimum performance.

The contributions to noise temperature ratio are the thermal noise of the series resistance, shot noise of the barrier, and flicker noise which is characteristic of the semiconductor. At intermediate frequencies in the MHz range, the major contribution is usually shot noise, but at lower frequencies flicker noise predominates. For mixer evaluation, the noise temperature ratio is the ratio of the noise actually produced under operating conditions to that thermal noise which would be produced by a resistor equal in magnitude to the output impedance of the mixer, at room temperature. It has been suggested (Ref. 4) that under conditions of d.c. excitation, in the limiting cases for an ideal Schottky barrier, the noise temperature ratio equals 1·0 for zero bias, tends to 0·5 for positive biases, and tends to values very much greater than 1·0 for negative biases. However, the theoretical problem of diode noise with local oscillator excitation is extremely complex, and no successful analysis has yet been accomplished.

Overall Noise Figure (MHz i.f.)

Current methods of mixer diode overall noise figure assessment are: measurement of conversion loss (using historical incremental methods) and noise temperature ratio, allowing calculation of overall noise figure performance from Eq. 6; or measurement of receiver overall noise figure using a calibrated broadband noise source. Experience has shown that the former method tends to give ambiguous results which cannot be achieved under actual operating conditions, whilst the latter method is preferred for absolute values and simulates operating conditions for performance referred to the mixer terminals. However, the use of a broadband noise source does imply that the noise power is available at both signal and image channels, hence the necessary addition of 3dB to the measured noise figure for the image matched value (sometimes termed single-sideband value). Image matched noise figure evaluation using a calibrated noise source has been used to characterise the mixer performance of devices discussed in this article.

Overall noise figure performances of the AAY39 and AEY17 as a function of frequency are illustrated in Fig. 5. The performance is quoted for a 45MHz 1·5dB i.f. amplifier. The noise figure results indicate that with use of the AAY39, overall receiver performances of 5·5dB at S-band (3GHz), 6·0dB at X-band (10GHz) and 7·0dB at J(Ku)-band (16·5GHz) are obtained. For the AEY17, a performance of about 8·0dB is achieved up to about 18GHz. Typical values of noise temperature ratio (i.f. = 45MHz) measured at X-band frequencies are about 1·1 and 1·4 for the AAY39 and AEY17 respectively, with conversion loss values of about 4·2 and 5·5dB respectively.

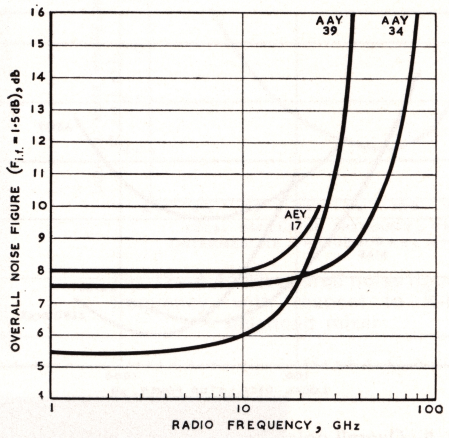

Fig. 5—Overall noise figure vs frequency

The measured noise figure performance of the AAY39 and AEY17 indicate good agreement between experimental and theoretical evidence regarding low frequency conversion loss (Table 1, Fig. 5). Further, degradation in performance with increased frequency is primarily due to the effect of the parasitics C_B and R_S.

The Q(Ka)-band diode AAY34 has been included in Fig. 5 for comparative purposes. This diode exhibits a greater cut-off frequency than the AAY39. This is a result of its higher design frequency and thus reduced value for the product of the spreading resistance and barrier capacitance. A receiver overall noise figure performance of about 8·5dB in conjunction with an i.f. amplifier of 1·5dB is thus indicated with use of the AAY34 at Q(Ka)-band frequencies. Typical values for conversion loss and noise temperature ratio (at 35GHz) are about 5·5dB and 1·6 respectively.

Operating Conditions

It may be worthwhile next considering the operating conditions to achieve optimum noise figure performance. Previously designed conventional point contact mixer diodes incorporating germanium usually require a small positive bias to obtain optimum performance, and their operation may be fairly critically dependent on local oscillator drive, bias, and load resistance (Refs. 6, 7). However, improved fabrication technology has reduced such effects for operation of the AAY39.

The X-band overall noise figure performance (45MHz 1·5dB i.f. amplifier) as a function of local oscillator power is illustrated in Fig. 6 for the AAY39 and AEY17. Optimum performance for the AAY39 is shown to occur at about 600μW for zero bias operation, which is equivalent to about 1mA rectified current. Further, the ability of the AAY39 to operate with reduced local oscillator drive is demonstrated, provided that a small positive bias is applied to the diode. Noise figure performance fairly independent of applied bias is illustrated for the AAY39 in Fig. 7, with a maximum load resistance of 150Ω.

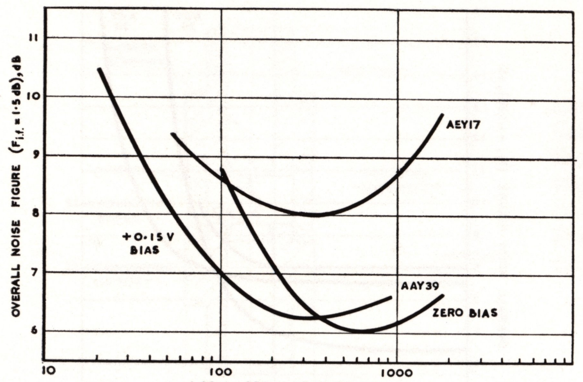

Fig. 6—Overall noise figure vs local oscillator power

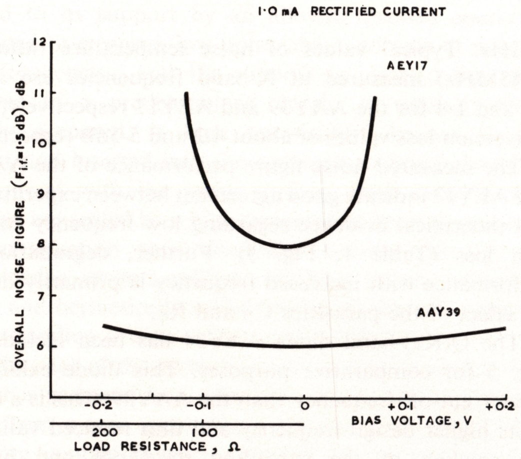

Fig. 7—Overall noise figure vs bias voltage

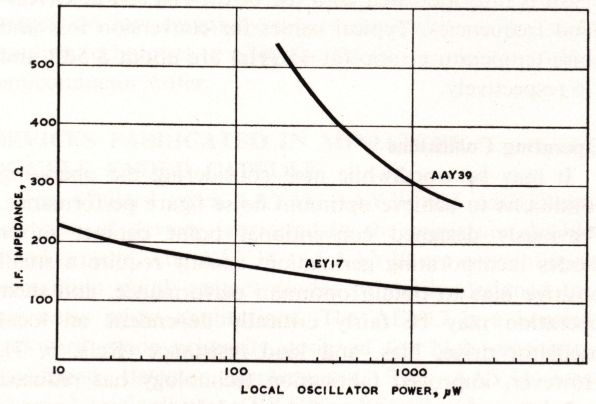

Fig. 8—I.F. impedance vs local oscillator power

The performance of the AEY17 under these operating conditions conforms to that expected from the I–V characteristics of a backward diode (Ref. 3). Optimum performance is obtained at about 200μW local oscillator power (Fig. 6), which is equivalent to about 1mA rectified current. The performance is, however, fairly critically dependent on drive, bias conditions, and load resistance (Figs. 6 and 7).

The i.f. impedance as a function of local oscillator power for the AAY39 and AEY17 is shown in Fig. 8. The i.f. impedance of the AAY39 at optimum operating conditions is about 350Ω, which is fairly typical for X-band mixer diodes. However, this value may be reduced by application of a small positive bias and increased local oscillator drive, still maintaining a commendably low noise figure performance. The low i.f. impedance obtained for zero bias operation of the AEY17 is illustrated.

The dynamic range of a mixer diode normally describes the linear dynamic range from threshold sensitivity to some higher value at which a prescribed degree of compression or departure from linearity occurs. The threshold sensitivity or lower level is determined by the receiver overall noise figure, whilst the upper level is determined primarily by the local oscillator power level. In the case of the conventional point contact diode, for example the AAY39, the 1dB compression point occurs at about −20dbm. However, as the result of the reduced local oscillator power requirements and I–V characteristic of the backward diode, the 1dB compression point occurs at about −30dbm for the AEY17.

R.F. Admittance

The good potential bandwidth properties of the AAY39 with an operating range into J(Ku)-band frequencies is illustrated in Fig. 9, which shows the r.f. admittance with respect to 0·02mho as a function of frequency. Theoretical r.f. admittance values calculated from Eq. 3 and Table 1 are included for comparative purposes, indicating the validity of the simple equivalent circuit, at least up to 14GHz. (Provision of a small positive bias will have the obvious advantage of improved bandwidth properties and match to 50Ω.)

For waveguide applications at X-band frequencies, the relatively high admittance of the AAY39 (Fig. 9) has to be accommodated in the waveguide mount design. The technique for test holders has been the use of reduced height waveguide mounts, and these are illustrated by Fig. 10, together with the collet method of holding the device. The waveguide height is reduced to $\frac{1}{16}$in. An r.f. bandwidth performance of about 30% centred at 9·5GHz is obtained with this design.

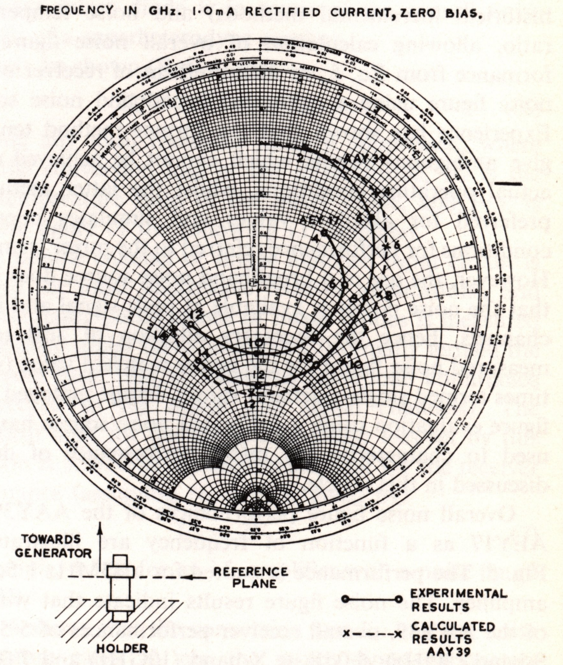

Fig. 9—AAY39, AEY17: r.f. admittance vs radio frequency (admittance with respect to 0·02mho)

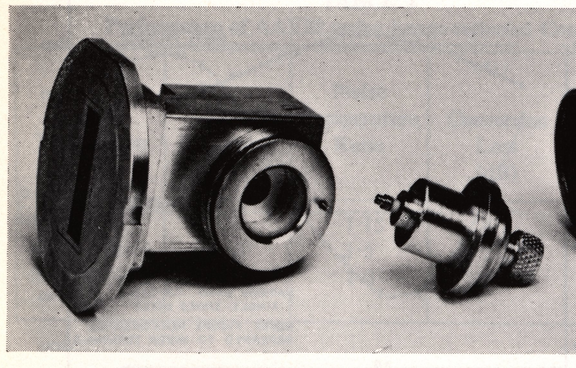

Fig. 10—AAY39: reduced height waveguide test mount

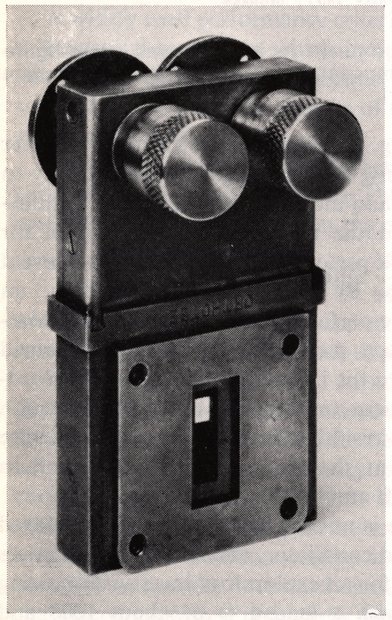

Fig. 11—AAY39: X-band balanced mixer CL7300

A balanced mixer based on the waveguide holder test mount is illustrated in Fig. 11. Overall noise figure performance as a function of frequency for the AAY39 with respect to this design is shown in Fig. 12.

An X-band printed strip line single ended mixer, formed by combining a 17dB coupler with a printed mount for the AAY39, is shown in Fig. 13. The r.f. bandwidth of this design is 8·6 to 10·6GHz, with isolation greater than 20dB.

The spread in r.f. admittance between samples of the AAY39 is controlled to extremely tight limits at a specified X-band frequency, such that the maximum v.s.w.r. is 1·33:1 with respect to a standard holder. Further, the spread in conversion loss is only about 0·5dB, thus ensuring reproducible devices for balanced mixer circuits, without selection of matched pairs.

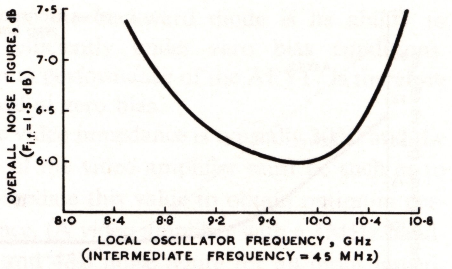

Fig. 12—AAY39: overall noise figure vs frequency, with respect to X-band balanced mixer

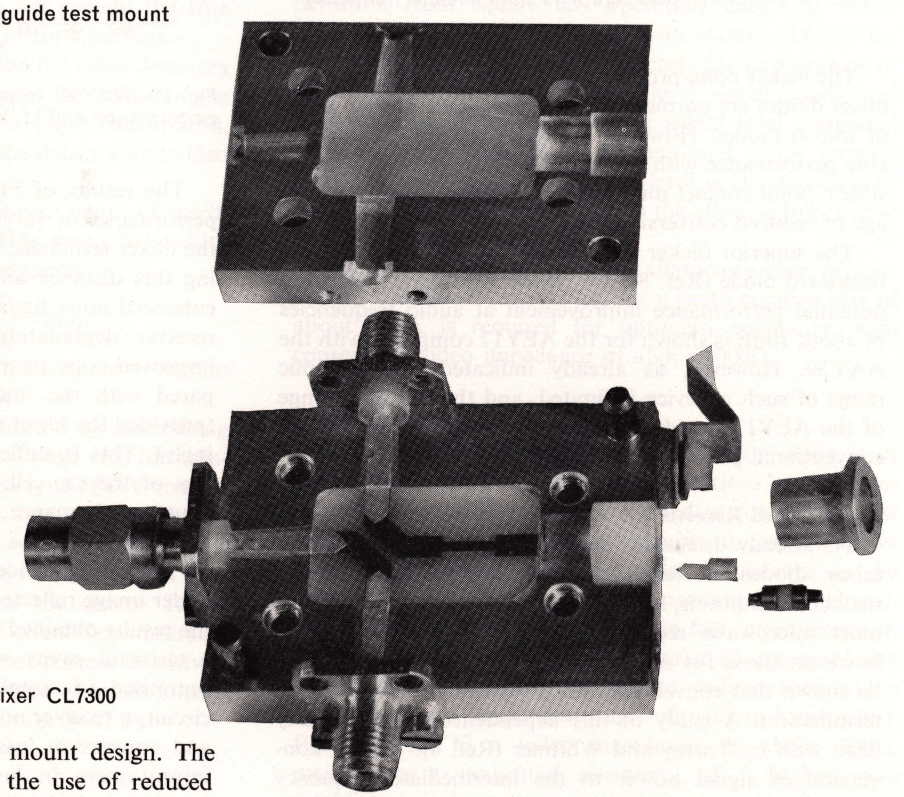

Fig. 13—AAY39: X-band printed stripline single ended mixer, $1\frac{1}{2}$ times actual size

The bandwidth properties of the AEY17 for mixer applications are also demonstrated in Fig. 9. With a local oscillator drive of about 200μW (that is, 1·0mA rectified current) the AEY17 has a maximum v.s.w.r. of 2·5:1 with respect to 50Ω at least over the measured frequency range 4 to 12GHz.

Overall Noise Figure (kHz i.f.)

The noise figure of any superheterodyne microwave receiver is dependent on the conversion loss and noise temperature ratio of the mixer diode. In general, the conversion loss is independent of the receiver intermediate frequency; but, because of the flicker noise contribution to the noise temperature ratio characteristic, the overall noise figure of the receiver deteriorates as the intermediate frequency is reduced. The flicker noise performances of the AAY39 and AEY17 are shown in Fig. 14, by illustrating receiver noise figure at X-band frequencies, as a function of intermediate frequencies.

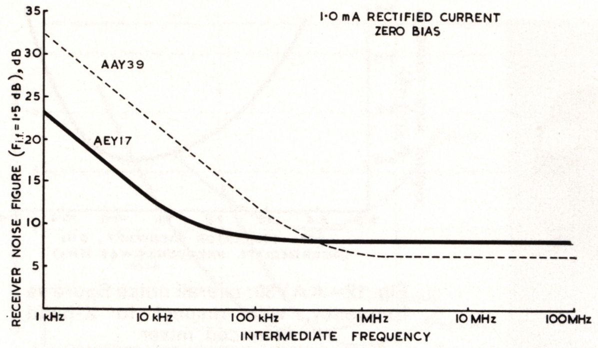

Fig. 14—Receiver noise figure vs intermediate frequency

The flicker noise properties of germanium point contact mixer diodes are normally expected to be worse than those of silicon diodes. However, the AAY39 exhibits comparable performance with the best available low flicker noise silicon point contact mixer diodes, with the added advantage of reduced conversion loss.

The superior flicker noise properties associated with a backward diode (Ref. 8), are clearly illustrated. In fact, a potential performance improvement at audio frequencies of about 10dB is shown for the AEY17 compared with the AAY39. However, as already indicated, the dynamic range of such a device is limited, and the dynamic range of the AEY17 is reduced by about 10dB compared with conventional point contact devices.

Image Tuned Receivers

As already discussed, the noise figure performance of mixer diodes is measured and specified under image matched conditions, and these conditions are favoured for most microwave receiver applications. These are not, however, those for minimum conversion loss, for it may be shown that conversion loss is dependent on the image termination. A study of this dependence has been fully dealt with by Torrey and Whitmer (Ref. 4). Briefly, conversion of signal power to the intermediate frequency entails the production of power at the image frequency. In the image-matched condition this power is dissipated in the image termination. However, if the power at the image frequency is reflected back into the mixer diode in the same voltage phase (that is, image open-circuit), this power may also be converted to the intermediate frequency. Accompanying this improvement in conversion efficiency there is an increase in the intermediate frequency impedance of the diode and the diode noise temperature ratio. Advantages of this effect may be considered under practical conditions in a radar receiver, for example, where the mixer diode is protected from the transmitter pulse by a narrow band t.r. cell. An investigation into such a receiver using the AAY39 is briefly summarised in Fig. 15. In this exercise, the parameters investigated were i.f. impedance and overall noise figure, and the investigation was carried out at X-band with an intermediate frequency of 45MHz. The resonant cavity used to tune the r.f. circuit was a narrow band t.r. cell with an insertion loss of 0·52dB, loaded Q of 130, and spike leakage of 0·04erg/spike.

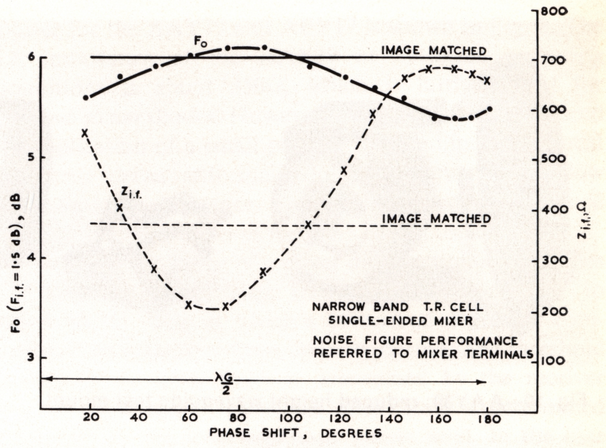

Fig. 15—AAY39: image tuned receiver. Overall noise figure performance and i.f. impedance vs phase of image reflection

The results of Fig. 15 illustrate the effect on receiver performance of varying the line length from the cavity to the mixer terminals, and indicate the necessity of optimising this distance and the i.f. amplifier input circuit for enhanced noise figure performance, or indeed, to prevent receiver degradation. By optimum line stretching, an improved noise figure performance of at least 0·5dB compared with the image matched conditions is obtained (provided the input to the i.f. amplifier is adjusted accordingly). This is sufficient to compensate for the insertion loss of the t.r. cell, resulting in a receiver overall noise figure performance at the mixer terminals better than 5·5dB for a 1·5dB i.f. amplifier.

This performance is not the best that may be achieved under image reflected conditions, and Table 2 summarises the results obtained for an exploratory investigation using a resonant cavity with a loaded Q of about 1000 and optimised i.f. amplifier input circuit. For image open-circuit, a receiver noise figure performance of about 5·0dB and conversion loss of about 2·0dB are indicated. The improvement in loss performance (compared with the image matched condition) is not, however, completely reflected in the overall noise figure performance because of the increase in the diode noise temperature ratio characteristic. The r.f. bandwidth of such a receiver obviously depends on the radio and intermediate frequencies and the loaded Q of the resonant cavity. In the above case the r.f. bandwidth was about 30MHz.

DETECTOR APPLICATIONS

The sensitivity of a video receiver is determined by a number of factors: the detector diode r.f. match, rectification efficiency, video impedance and noise properties, together with the video amplifier noise figure and bandwidth. The quality of the video detector diode can be expressed quantitatively in terms of short circuit current sensitivity (rectification efficiency) and video impedance, by the 'figure of merit', which may be defined by:

$$M = \beta Z_V^{\frac{1}{2}} \quad \ldots(8)$$

where β is the microwave short circuit sensitivity and Z_V is the video impedance.

However, the expression does not include the noise properties of the detector and does not present the true quality of devices under conditions of forward bias.

TABLE 2
Performance of AAY39 under Image-reflected Conditions

Image Termination	I.F. Impedance (Ω)	Noise Temperature Ratio	Conversion Loss (dB)	Overall Noise Figure ($F_{i.f.} = 1{\cdot}5$dB) (dB)
Match	350	1·15	4·2	6·0
Open-circuit	850	1·5	2·2	4·9
Short-circuit	220	1·0	4·7	6·2

A widely used performance criterion for video detectors is 'tangential sensitivity' which indicates the ability of the detector to detect a signal against a noise background, and includes the noise properties of the detector and video amplifier (Ref. 9).

An approximate relationship between 'figure of merit' and tangential sensitivity for a 1MHz video bandwidth may be derived (Ref. 10) from the equation:

$$T_s = \left(51 + 10 \log_{10} \frac{M}{60}\right) - \text{dbm}$$

which implies that a tangential sensitivity of −51dbm corresponds to a figure of merit of 60.

For detector applications, in addition to minimising the parasitics C_B and R_S (discussed on page 123) for satisfactory microwave operation, the best type of I–V characteristic for rectification efficiency is one with maximum curvature at the operating point. It is desirable that this should occur at zero bias, as the use of bias current may introduce some additional noise into the system. It has been shown that the backward diode offers these desirable characteristics with a potentially higher current sensitivity performance coupled with a lower value of video impedance than a conventional detector diode (Ref. 3).

Low Level Sensitivity

With use of the AEY17, a zero bias tangential sensitivity performance of about −54dbm (4dB, 1MHz bandwidth video amplifier) may be achieved independent of radio frequency up to about 18GHz. For a video impedance of 300Ω, characteristic of the AEY17, it may be shown that this value approaches very closely the theoretical low frequency value of −56dbm (Ref. 11). Measurements of short circuit current sensitivity at X-band frequencies and video impedance indicate typical values of 8μA/μW and 300Ω respectively, with a resultant 'figure of merit' of about 150.

For the AAY39, a tangential sensitivity performance of about −52dbm (2dB, 1MHz bandwidth video amplifier) may be obtained up to about 10GHz. The sensitivity is comparable with the performance of the best conventional point contact diode available.

Operating Conditions

It has been shown that no practical advantage in sensitivity performance is obtained by biasing a backward diode (Ref. 3). In fact, as already discussed, one of the chief merits of the backward diode is its ability to detect efficiently under zero bias conditions. Optimum performance of the AEY17 is therefore obtained at zero bias.

The video impedance is typically 300Ω and the design of the video amplifier must be such as to accommodate this value to obtain optimum performance. (A video amplifier with a 1MHz bandwidth and 4dB noise figure for an input impedance of 300Ω was used to characterise the performance of the AEY17.)

At low level (or square law) signal conditions, 1dB deviation from square law operation occurs at about −23dbm signal level, compared with about −18dbm for a conventional point contact detector (for large values of video load resistance). At high level signal conditions, saturation occurs at about 0dbm signal level compared with about 20dbm for a conventional point contact detector. The reduced saturation level is characteristic of the backward diode and is due to the effective low reverse voltage breakdown encountered.

The AAY39 conforms to the characterisation of conventional detector diodes. That is, a small positive bias of about 50μA is required for optimum sensitivity, with consequent video impedance of about 1000Ω.

R.F. Admittance

The microwave bandwidth of a detector diode is of significant importance for many applications, and a compromise of sensitivity may be required to achieve the best overall performance. It is reasonable to expect better bandwidths for low values of video impedance as the relative effect of the barrier capacitance is reduced. (Conventional detector diodes are, in fact, often biased in the forward direction, not only to take advantage of any improvement in sensitivity, but to reduce their video impedance with consequent improvements in bandwidth). For the AEY17 a video impedance of about 300Ω, maintaining a tangential sensitivity of −54dbm, was established as the design criterion.

The broadband qualities of the AEY17 are illustrated in Fig. 16, which shows the r.f. admittance with respect to 0·02mho as a function of frequency. The admittance spread between samples is controlled to extremely tight limits at a specified X-band test frequency, ensuring reproducibility of device parameters.

To demonstrate the validity of the simple equivalent circuit, theoretical r.f. admittance figures calculated from Eq. 3 and Table 2 are included in Fig. 16 for comparison.

ADAPTATION OF THE MINIATURE CAPSULE

It has already been indicated that the small size of the miniature double ended capsule lends itself to mechanical adaptation to standard outlines. Fig. 17 illustrates the adaptation to the coaxial outlines of the X-band SIM2/5 and J-band 1N78 types. Design of coaxial adaptors for these frequencies has also maintained the required r.f. admittance so that the improved performance of the AAY39 and AEY17 may be offered for existing equipments. For example, the Mullard types AAY50 and

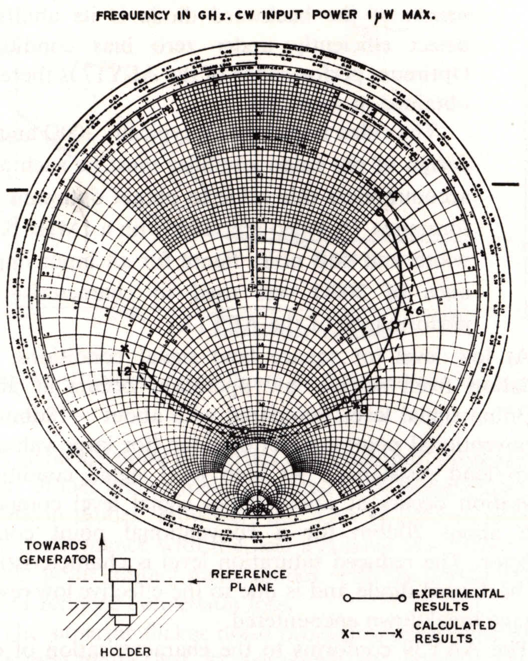

Fig. 16—AEY17: r.f. admittance vs radio frequency (admittance with respect to 0·02mho)

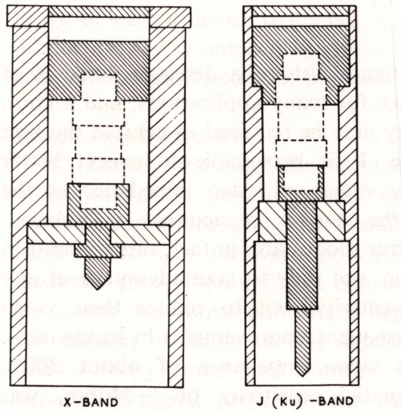

Fig. 17—Adaptation of miniature capsule to coaxial outlines

AAY50R have been designed specifically as retrofits for X-band coaxial outline devices, and the Mullard types AAY51 and AAY51R have been designed specifically as J(Ku)-band coaxial outline devices.

The typical overall noise figure performance for the AAY50/50R of 6·2dB, in conjunction with a 1·5dB i.f. amplifier, indicates that improved receiver performance of about 1·5dB compared with existing X-band coaxial mixer diodes may be achieved.

The AAY51/51R overall noise figure performance of about 6·7dB ($F_{i.f.} = 1{\cdot}5$dB) measured at 13·5GHz again indicates a potential improvement in receiver performance at J(Ku)-band frequencies compared with the 1N78 types. Further, the adaptor design maintains the inherent broadband properties of the AAY39; for mixer applications a maximum v.s.w.r. of 2·5:1 with respect to 68Ω is achieved, over the frequency range of 12·5 to 18GHz.

Adaptation of the AEY17 into coaxial outlines may also achieve high sensitivity broadband performance for detector applications, eliminating the complications incurred with bias circuits necessary for conventional detector diodes. For example, the AEY29 is designed for the J(Ku) band.

BURNOUT PERFORMANCE

Microwave diodes may be damaged in a variety of ways resulting in a deterioration of sensitivity; when by common usage, they are said to be burnt out.

The physical cause of diode burnout is complicated, but it is usually accepted that burnout is the result of high temperatures produced at the junction leading to diffusion or melting. The thermal time constant of the diode determines whether the heat generated is proportional to the energy or the total power dissipated. It is customary to specify burnout ratings for mixer diodes (where overloads encountered normally consist of nanosecond pulses due to t.r. cell leakage) in spike energy, and for detector diodes (where overloads normally consist of microsecond pulses) in peak pulse power.

There are inherent difficulties in measuring absorbed power or energy from microwave pulses, and this leads to burnout ratings being specified in terms of r.f. incident power or d.c. spike and pulse generation methods. Under r.f. conditions, the dissipated power in the diode may only be a fraction of that available, depending on the amount of self protection afforded by the r.f. mismatch of the diode at high levels of power. This action may be compared with that of a limiter, where the power reflected (or isolation) is a function of the transmission line characteristic impedance. Hence, the diode r.f. impedance at operating power level may have significant effect on the dissipated power and thus apparent burnout performance.

In the case of t.r. cell spike leakage, the duration of the spike is a few nanoseconds; the spike has a very broad frequency spectrum, so that the bandwidth of the r.f. circuit following the t.r. cell may have important implications on the energy/pulse delivered to the diode. Further, the measured spike energy is usually an average of a number of pulses; but a single spike of abnormal energy may be the sole cause of diode burnout. T.R. cell spike leakage may be simulated by d.c. spikes produced by a coaxial line discharge, and as the consistency between spikes produced in this manner is believed to be greater than between t.r. cell leakage spikes, d.c. spike burnout tests are often preferred to assess burnout properties of mixer diodes. Unfortunately, however, a good correlation between r.f. and d.c. performance has not yet been fully established, and there is experimental evidence to show that d.c. burnout level is dependent on the number of applied spikes. As an example, Fig. 18 illustrates the dependence obtained for the AAY39 and shows quite clearly that the energy level for a large number of spikes is far more deleterious than a single spike of the same energy. Further, the shape of the curve is dependent on the diode type, and experience has shown that evaluation by d.c. methods (for a limited number of spikes) does not ensure compatibility of a t.r. cell type with a mixer diode type. Hence, both r.f. and d.c. methods of burnout assessment have severe limitations, and although r.f. assessment under controlled conditions gives the most reliable information for system design, comparative data tend to be rather ambiguous unless the r.f. circuit conditions are carefully defined. With the advent of solid state limiters, however, the spike leakage can be sufficiently small to reduce mixer diode burnout problems (due to the magnetron pulse) under any circuit conditions, and these should give greatly increased receiver reliability. T.R. cell varactor limiters can already reduce the spike leakage to about 0·01erg/spike at X-band.

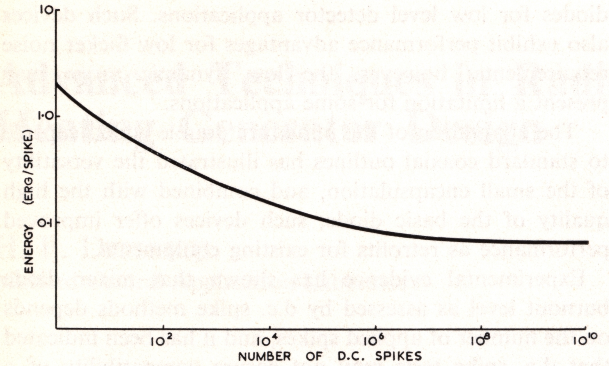

Fig. 18—AAY39: burnout vs number of d.c. spikes

In the case of diode burnout as the result of r.f. microsecond pulses, it is normal practice to apply a short duration test (about 10 minutes). However, experience has indicated that continuous operation, say in excess of 100 hours, reduces the power level at which deterioration occurs by a factor of about 10:1.

The definition of criterion for burnout is not always very explicit. In the following results, a 1dB or greater change in noise figure performance was used for mixer evaluation, and a minimum figure of merit of 120 was applied for evaluation of the AEY17 for detector applications. A burnout level implies a level for 90% survival.

The burnout properties of the AAY39 have been assessed at X-band frequencies with single ended mixers, in conjunction with narrowband and broadband t.r. cells and under conditions of r.f. microsecond pulse power.

The tests in conjunction with broadband t.r. cells have emphasised the important influence of the bandwidth of the r.f. circuit following the t.r. cell on the protection afforded by the t.r. cell. The experimental evidence is summarised in Fig. 19. Briefly, the results indicate that the burnout of the AAY39, when used in conjunction with its broadband waveguide test mount (30% r.f. bandwidth), appears inferior to the burnout when the AAY39 is adapted to the AAY50 coaxial outline and used in conjunction with its bar and post type mount (10% r.f. bandwidth). Again, the protection may be further improved by restricting the r.f. bandwidth by use of a narrowband filter (about 3% r.f. bandwidth). It is of interest to note the agreement in burnout level between r.f. and d.c. tests in the limiting cases; that is, about 0·065erg/spike (Figs. 18 and 19). Tests in conjunction with narrowband t.r. cells (spike leakage 0·04erg/spike) and the broadband waveguide mount have indicated satisfactory life performance for these diodes. Further, measurement of dynamic noise figure has shown that no temporary deterioration in noise figure performance, after incident pulses, is experienced under these conditions. Results of pulse burnout tests (pulse width 0·5μs, repetition rate 2000p/s) in conjunction with the two different types of mount (waveguide and coaxial), have indicated burnout ratings of about 0·8W peak power for the waveguide mount and about 3W peak for the coaxial mount (AAY50).

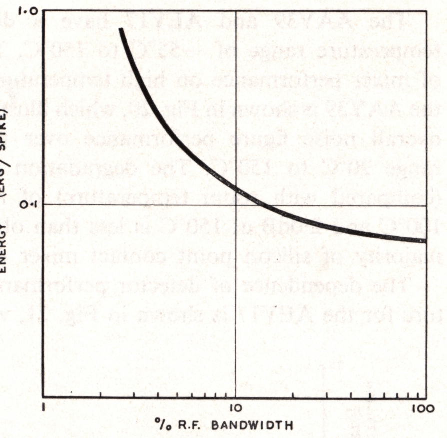

Fig. 19—AAY39: t.r. cell leakage burnout performance

Extensive t.r. cell leakage tests have not yet been carried out on the AEY17, but initial results at X-band frequencies have indicated a burnout level of about 0·05erg/spike for broadband applications. This implies the need for the protection offered by a t.r. cell varactor limiter device. Results of pulse burnout tests (pulse width 0·5μs, repetition rate 2000p/s) indicate a burnout level of about 0·7W peak power for short periods, whilst long term tests have established a safe design limit of 50mW peak power for continuous operation.

TEMPERATURE DEPENDENCE

It is traditionally assumed that germanium devices have a poorer performance at elevated temperatures when compared with silicon devices. This is not true for the very heavily doped semiconductor materials used for microwave point contact diodes. Further, backward diodes may be expected to be even less temperature dependent (Ref. 8).

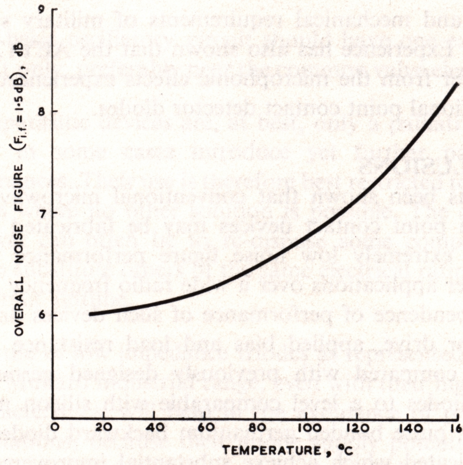

Fig. 20—AAY39: overall noise figure vs temperature

The AAY39 and AEY17 have a design operating temperature range of −55°C to 150°C. The dependence of mixer performance on high temperature operation for the AAY39 is shown in Fig. 20, which illustrates the typical overall noise figure performance over the temperature range 20°C to 150°C. The degradation in performance (compared with room temperature) of about 0·8dB at 100°C and 2·0dB at 150°C is less than obtained with the majority of silicon point contact mixer diodes.

The dependence of detector performance on temperature for the AEY17 is shown in Fig. 21, which illustrates video impedance and tangential sensitivity performance over the temperature range 20°C to 150°C. The degradation in tangential sensitivity is due mainly to the change in video impedance.

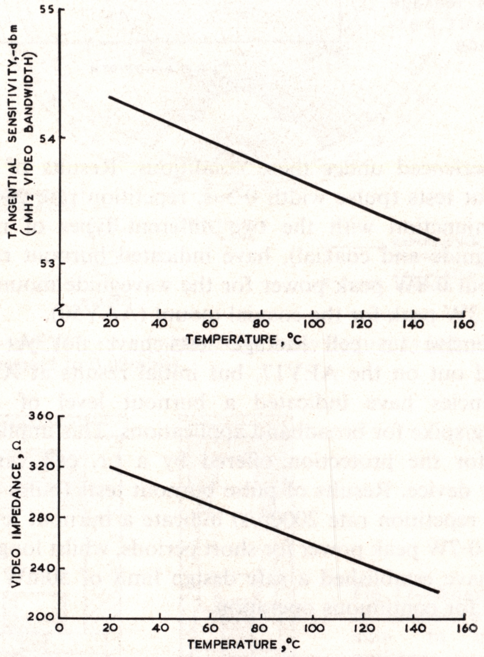

Fig. 21—AEY17: low level detector performance as a function of temperature

MECHANICAL PERFORMANCE

The AAY39 and AEY17 meet the normal environmental and mechanical requirements of military specifications. Experience has also shown that the AEY17 does not suffer from the microphonic effects experienced with conventional point contact detector diodes.

CONCLUSIONS

It has been shown that conventional microwave germanium point contact devices may be fabricated which achieve extremely low noise figure performance values for mixer applications over a wide radio frequency range. The dependence of performance of such devices on local oscillator drive, applied bias and load resistance is improved compared with previously designed germanium mixer diodes to a level comparable with silicon mixers. Further, pulse bonded germanium backward diodes may be fabricated which achieve substantial improvement in performance compared with conventional point contact diodes for low level detector applications. Such devices also exhibit performance advantages for low flicker noise requirements; however, the low dynamic range may present a limitation for some applications.

The adaptation of the miniature double ended capsule to standard coaxial outlines has illustrated the versatility of the small encapsulation, and combined with the high quality of the basic diode, such devices offer improved performance as retrofits for existing equipments.

Experimental evidence has shown that mixer diode burnout level as assessed by d.c. spike methods depends on the number of applied spikes, and it has been indicated that d.c. spike tests may not ensure compatibility of a mixer diode type with a t.r. cell type. Further, the effect of the r.f. circuit on r.f. burnout performance has been illustrated.

Finally, it has been shown that both the germanium point contact diode and bonded backward diode, fabricated in the rugged double ended capsule, have an operating temperature range up to 150°C.

ACKNOWLEDGEMENTS

This work was supported by the Ministry of Defence, whose permission to publish this paper is acknowledged.

The author wishes to acknowledge the support of his colleagues at the Hirst Research Centre, A.S.M. Stockport, and Mullard Research Laboratories for device design, fabrication, and performance evaluation.

REFERENCES

1. Meredith, R. and Warner, F. L. 'Superheterodyne Radiometers for use at 70Gc and 140Gc'. **IEEE Trans on Microwave Theory and Techniques,** Vol. MTT-11, No. 5, Sept. 1963, pp. 397 to 411.
2. Oxley, T. H. and Summers, J. G. 'Metal-Gallium Arsenide Diodes as Mixers'. **Inst. Phys. and Phys. Soc. Conf. Ser.** No. 3: Gallium Arsenide, 1966. paper No. 19, pp. 138 to 150.
3. Oxley, T. H. and Hilsden, F. 'The Performance of Backward Diodes as Mixers and Detectors at Microwave Frequencies'. **Jour. IERE (Radio and Electronic Engineer),** Vol. 31, No. 3, Mar. 1966, pp. 181 to 191.
4. Torrey, H. C. and Whitmer, C. A. 'Crystal Rectifiers'. **MIT Radiation Lab. Ser.** No. 15. McGraw-Hill, 1948.
5. Southworth, G. C. 'Principles and Applications of Waveguide Transmission', chap. 12. D. van Nostrand, 1950.
6. Messenger, G. C. and McCoy, C. T. 'A Low Noise-figure Microwave Crystal Diode'. **IRE Convention Record,** Part 8, 1955, pp. 68 to 73.
7. Lindell, A. O. and Oxley, T. H. 'Radar Crystal Valves'. **Proc. IEE,** Vol. 106, Part B, Supp. 15, May 1959, pp. 426 to 433.
8. Eng, S. T. 'Low-noise Properties of Microwave Backward Diodes'. **Trans IRE on Microwave Theory and Techniques,** Vol. MTT-9, No. 5, Sept. 1961, pp. 419 to 425.
9. Lucas, W. J. 'Tangential Sensitivity of a Detector Video System with R.F. Preamplification'. **Proc. IEE,** Vol. 113, No. 8, Aug. 1966, pp. 1321 to 1330.
10. Frohmaier, J. H. 'Noise Performance of a Three-stage Microwave Receiver'. **Electronic Technology,** Vol. 37, No. 6, June 1960, pp. 245 to 246 (letter to the editor).
11. Shurmer, H. V. 'Backward Diodes as Microwave Detectors'. **Proc. IEE,** Vol. 111, No. 9, Sept. 1964, pp. 1511 to 1516.

Advanced Techniques in Radio Frequency Heating Generator Design

H. F. Dittrich
Mullard Central Application Laboratory

Radio frequency heating generators, for either dielectric or induction heating, can be made efficient and stable by observing the design criteria enumerated in this article.

INTRODUCTION

The use of radio frequency power generators for dielectric and induction heating purposes is a well established and rapidly growing branch of industrial electronics. By far the largest proportion of these generators use thermionic triodes as energy converters at frequencies ranging from 100kHz to several hundred MHz, and at power levels of 500W to 500kW. Since the large majority of these equipments are self-oscillating generators and are, moreover, subject to large reactive and resistive load variations, there are valve problems and circuit problems which are distinctly different from those in driven amplifiers.

The use of modern valves and components, specifically designed for industrial usage, in combination with advanced circuit techniques, can help to overcome these difficulties and will lead to more elegant and therefore more efficient and stable constructions.

DESIGN CRITERIA

The design examples presented in the following three articles (Refs. 1, 2 and 3), though treating three separate projects, are linked by a common circuit design philosophy; that is, to prevent rather than cure parasitic oscillations, and maintain a high circuit efficiency. The main criteria embodied in this design philosophy may be summarised in the following points:

1) The ideal circuit should contain only those components that are essential to the basic oscillatory function.

2) Since difficulties arise, not so much with the generation of the required frequency, but rather in trying to avoid moding or parasitic oscillations, the use of v.h.f. techniques is recommended in the construction of generators operating even at frequencies as low as 100kHz.

3) To satisfy the demands made in points 1 and 2 it is necessary to construct circuits with well defined capacitive and inductive components that have a minimum of stray reactances. The physical outline and connecting facilities of these components are therefore as important as their electrical rating, and because r.f. currents travel largely along surfaces, the full electrical integration of the components into the circuit will only be possible if a good structural integration has been achieved.

4) Since, in terms of circuitry, the valve is a capacitive element, its satisfactory integration with the remaining circuit capacitance becomes imperative. This will, in many cases, only be possible with valves of coaxial construction, such as the Mullard valves shown in Fig. 1.

5) For de-coupling and filtering purposes, use is made, wherever possible, of the natural r.f. potential gradients along the outline of the basic oscillatory components. The use of filtering chokes and capacitors can thereby be largely avoided, thus further reducing the incidence of stray resonances.

6) The functions of tank, feedback and load circuits should be electrically well separated so that there will be less chance of stray coupling through common parasitic paths.

7) The basic oscillatory circuit should have one earthing point only, preferably near the common valve electrode.

8) Antiparasitic devices are, at best, only a palliative and may in some cases introduce yet further parasitic resonances. Their use is therefore best restricted to those cases where no other solution is possible. The correct answer can often be to re-dispose some components or to substitute others of the same electrical ratings but different outline.

9) The use of low impedance triodes as represented in the new Mullard industrial range, even with their high gain characteristics, will help in the avoidance of parasitic oscillations, because their anode supply potential and the resultant r.f. swing are also relatively low.

Whilst the loaded Q of the fundamental frequency

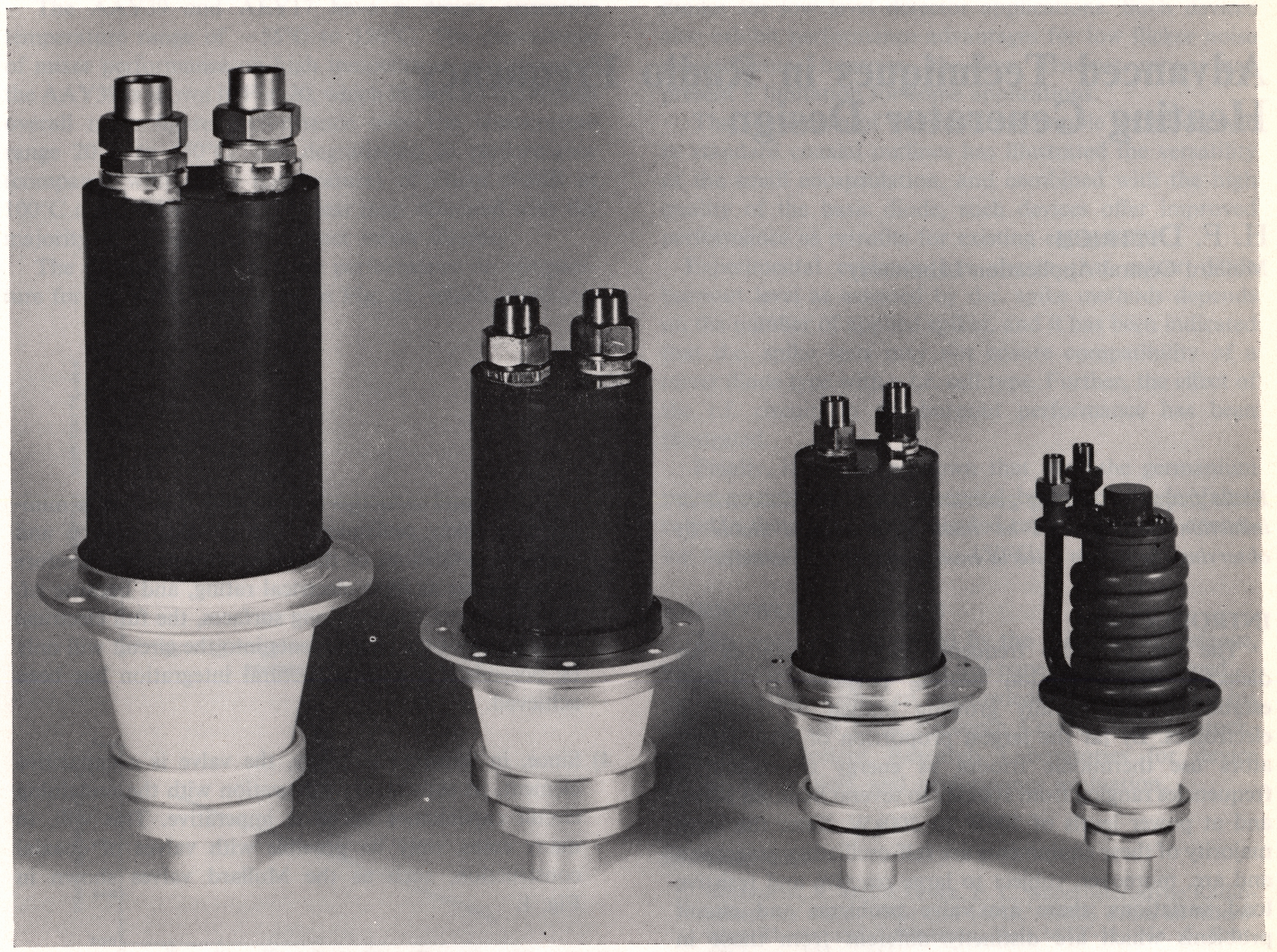

controlling circuit can be made to have any desired value by apportioning the necessary C and L values to the appropriate components, the loaded Q of incidental parasitic resonators is kept lower when a low voltage supply and a lower anode swing are applied. For any given layout, the stray C/L values of the parasitic resonators will be constant, but their Q and, therefore, their ability to generate parasitic oscillations will rise with the square of the applied potential.

An upward transformation of the generated r.f. potential to the load position can, if necessary, be obtained by suitable load circuit arrangements that will not affect the operation of the basic oscillatory circuit.

Fig. 1—Typical Mullard water-cooled ceramic envelope industrial triode valves. From left to right the valves are YD1212, YD1192, YD1182, YD1172. Valves are shown approximately one fifth actual size.

REFERENCES

1. DITTRICH, H. F., 'Dielectric Heater Using Half-wave Line at 30MHz.' **Mullard Technical Communications,** Vol. 10, No. 94, July 1968, pp 135 to 145.
2. NIGHTINGALE, D. E., 'A 400kHz Induction Heater of Advanced Design for Powers up to 60kW.' **Mullard Technical Communications,** Vol. 10, No. 94, July 1968, pp. 146 to 149.
3. NIGHTINGALE, D. E., 'A 300kHz Induction Heater of Advanced Design for Powers up to 120kW/240kW.' **Mullard Technical Communications,** Vol. 10, No. 94, July 1968, pp. 150 to 156.

Dielectric Heater Using Half-wave Line At 30MHz

H. F. DITTRICH
Mullard Central Application Laboratory

Details are given of a 30MHz dielectric heater using a half-wave line to couple the generator to the load. Advantages over the more conventional quarter-wave line coupling are improved load-power to processing-time relationship, greater stability of the oscillator and comparative simplicity of design. Load powers developed are 14·5kW with the YD1172 triode and 28·5kW with the YD1182.

INTRODUCTION

The pre-heating of modern plastic materials requires the application of radio frequency energy at high potential differences across the work material. Whilst the design of r.f. power oscillators to meet these requirements is basically simple, difficulties caused by parasitic resonances and moding are often experienced in practice. The generator-load-circuit described in this article shows distinct advantages over more conventional techniques in being simple in construction and remarkably free from spurious resonances.

PROCESSING REQUIREMENTS

A good estimation of the processing conditions in a dielectric heater may be made from the dielectric loss formula

$$P_W = V^2 \pi \varepsilon' f \tan\delta \qquad \ldots(1)$$

where

P_W = power absorbed by a unit volume of work material
V = applied peak r.f. potential difference
ε' = capacitance per unit volume
f = processing frequency
$\tan\delta$ = loss factor.

It may be seen that for any given material and operating frequency the only variable influencing the equipment design is the applied r.f. potential difference. With the loss factor of many of the materials to be treated extending only into the second decimal of tan δ, it is desirable, therefore, to have the highest possible load potential difference for the longest possible part of the processing time. This means that the load should, for this period, appear to be as nearly as possible purely resistive.

A graph comparing the usual loading characteristic with an ideal one is shown in Fig. 1: it can be deduced from Fig. 1 that substantial equipment economies, or processing improvements, can be made if the ideal power-time distribution is approached. The curve (a) is for a load-coupling circuit that contains reactive components, which may be partly in the load material; it is a 'tuning' characteristic and places a high peak power demand on the generator. Curve (b) is for a coupling that is resistive throughout the processing time: changes in load power are then caused solely by changes in tan δ in the load material. A considerable saving in process time or peak power rating of the equipment can be achieved with characteristic (b).

CONVENTIONAL CIRCUITS

Since the dimensions of the load material in a pre-heater are usually small in comparison with the operating wavelength, potential distribution patterns present no problem and the choice of operating frequency is governed by, inter alia, the maximum permissible frequency for a given valve type at full d.c. input. This will then, with most valves of industrially attractive power levels, lie between 30 and 160MHz. Although r.f. potential differences of the right order may be obtained with conventional circuit techniques at the valve anode, difficulties are often met when a direct or step up transfer of this potential difference to the load position is attempted.

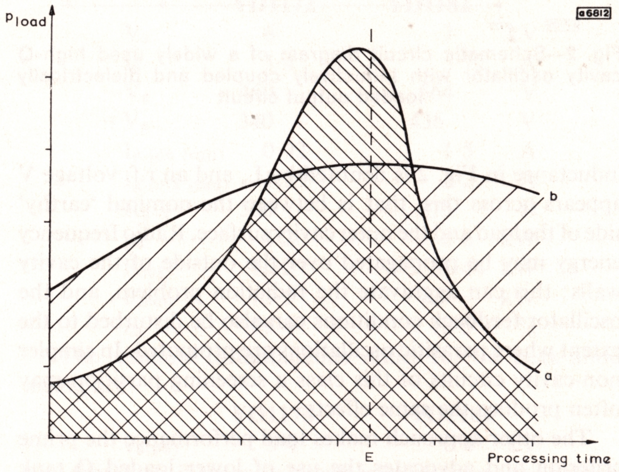

Fig. 1—Comparison of load-power distribution over the processing-time obtained with two different load circuit systems. Curve (a) relates to a circuit and load that contains reactive components. Curve (b) relates to a circuit and load that appears entirely resistive

Two distinct design approaches have consequently crystallized in common practice. One approach places the emphasis on stable operation within well defined narrow frequency bands, and freedom from harmonic frequencies, but carries as a penalty a poor time-integrated load power transfer that is most noticeable with materials that change their electrical properties during the processing cycle (Fig. 1). To compensate for the consequent mismatches within a given processing time, the nominal power level of the generator is then often required to be far in excess of the real processing needs. Moreover, the tank circuits employed for this class of generator are of the high loaded Q type, and usually have some form of cavity with an inductive load coupling (Fig. 2). During periods of detuning the load circuit will change its earth potential reference with respect to the tank circuit as follows: lead inductance in Fig. 2 is denoted by L, and an r.f. voltage V appears across this, that is between the nominal 'earthy' side of the load and the outer cavity surface. Radio frequency energy may be propagated over the outside of the cavity walls: this can aggravate the radiation problem, and the oscillator feedback conditions can also be disturbed to the extent where parasitic oscillations are promoted. In simpler non-cavity circuits of this class a screening partition may often produce the same effects.

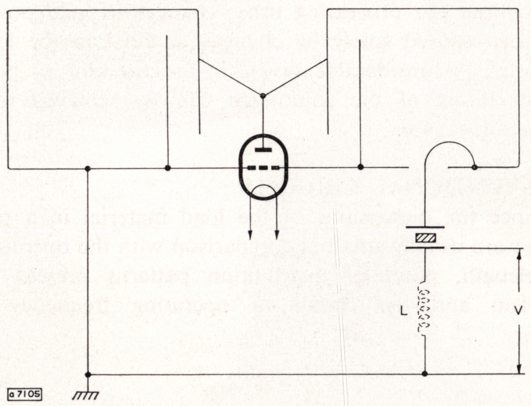

Fig. 2—Schematic circuit diagram of a widely used high-Q cavity oscillator with inductively coupled and dielectrically loaded output circuit

The other approach makes load performance the prime criterion and advocates the use of lower loaded Q tank circuits and tight coupling so that the oscillator frequency may be pulled a certain amount with changes in load reactance, resulting in a fairly constant power transfer. Over-wound tank inductors together with capacitive or even direct coupling are often used. At the frequencies and power levels concerned, valve and circuit stray reactances can easily be of a similar Q value to that of the main tank circuit components, and may cause oscillations of their own resonance to be generated.

Fig. 3 shows the essential components of such a circuit and since the connections between these must be interpreted as being of finite dimensions and having electrical properties, it may be seen that at least three possible parasitic circuits exist. The generator anode circuit has an over-wound (auto transformer) tank coil, and generator tank capacitance C_G and tank inductance L_G are intended as the frequency controlling elements, but it is obvious that other circuit paths are possible: one is c_{a-f} of the valve with C_G, and the connecting leads L_C as complementary inductor; another is c_{a-f} with inductor L_T of the transformer section and the coupling capacitor C_C and work material capacitance C_W; another is via L_G, L_T, C_C and C_W. The grid and feedback circuits, deliberately omitted in Fig. 3, would further increase the parasitic permutations. Similar circumstances will obtain if L_T is assumed to be the lead inductance between the tank circuit and the load coupling capacitor. It is also evident that, in the example given in Fig. 3, these circuits have a common reference point and may in the presence of feedback, whether intentional or stray, be excited into violent oscillations.

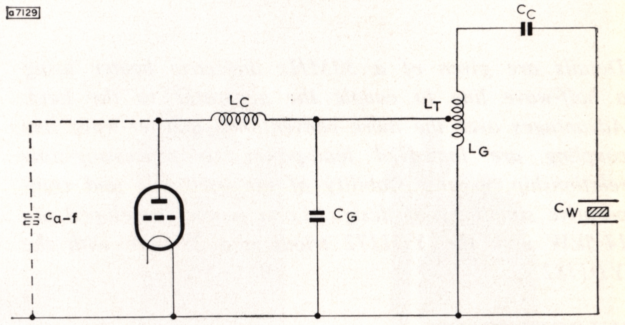

Fig. 3—Low Q_L tank circuit

THE HALF-WAVE LINE OSCILLATOR

A number of desirable attributes for a new circuit design emerge from the shortcomings mentioned in the previous paragraph.

1) The basic oscillatory-load circuit should have one resonance only.
2) Transformation, preferably upward from the r.f. anode potential, should be possible.
3) Reactive changes in the load should not cause parasitic oscillations.
4) There should be no r.f. partitioning between the tank and load circuits.
5) Maximum possible coupling of the load should be maintained over the whole of the processing cycle.

A single r.f. circuit is therefore required that will, at its natural frequency, exhibit two r.f. voltage maxima, representing the generator voltage and load voltage.

A half-wave line appears to satisfy this condition. If this line is then shortened by end-loading capacitors representing the generator valve and tank circuit capacitance on one end, and the load capacitance on the other, there exists the possibility of achieving a voltage transformation along the line proportional to these end-loading capacitances.

The voltage distribution along such a line is shown in Fig. 4 where it is assumed that the generator end capacitance C_G is larger than the load capacitance C_L. The voltage minimum will always be positioned one electrical quarter wavelength from each end, and move physically along the line as the ratio of these capacitances is changed. The transformation ratio is derived as follows.

Since both line sections have the same characteristic impedance, we may write

$$V_G \sin\theta_L = V_L \sin\theta_G. \qquad \ldots(2)$$

The transformation ratio will be

$$T = \frac{V_L}{V_G} = \frac{\sin\theta_L}{\sin\theta_G}, \qquad \ldots(3)$$

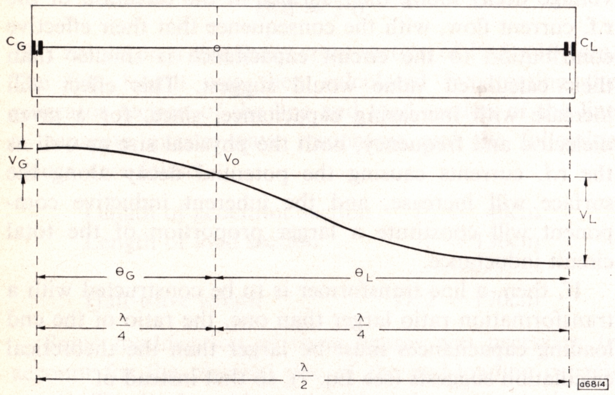

Fig. 4—Voltage distribution along a half-wave line with capacitive ends

where θ_G and θ_L are the respective lengths of the shortened line in radians. The value of θ may be calculated from the equation for a capacitively loaded line, where the physical line length is given by

$$\ell = \lambda\frac{\theta}{2\pi}, \qquad \ldots(4)$$

and θ is related to the circuit constants by

$$\tan\theta = \frac{\lambda}{2\pi v C Z_o} \qquad \ldots(5)$$

in which v is the velocity of light, C is the end-loading capacitance and Z_o is the characteristic line impedance. However,

$$\tan\theta = \frac{\sin\theta}{\cos\theta}, \qquad \ldots(6)$$

and so the transformation ratio can also be related directly to the end-loading capacitances by the equation

$$T = \frac{C_G\cos\theta_L}{C_L\cos\theta_G}. \qquad \ldots(7)$$

A variation of load reactance will thus slightly change the transformation ratio and frequency but will not affect the load coupling greatly because the load always appears resistive. By such means unity coupling is maintained throughout the processing cycle and any variation of power transferred to the load is mainly caused by a change in tan δ.

The likelihood of parasitic oscillations is also greatly reduced as any reactive changes that are normally reflected into a quarter-wave tank circuit, causing incorrect feedback conditions through common tank and drive circuit connections, are taken up by the floating zero-point on the half-wave line.

There is no r.f. partitioning between generator and load position since each is part of one integral circuit. The half-wave system therefore is singularly suitable for pre-heating and process drying in the v.h.f. range.

DESIGN OF PROTOTYPE

A general purpose dielectric heater operating at 30MHz and suitable for the pre-heating of plastics or process drying is now described. The circuit is so arranged that the nominal power level would be 15kW when fitted with the YD1172 or 30kW with the YD1182.

Since for a given frequency the required heating losses in a dielectric load material are proportionate to the square of the applied r.f. voltage, it was decided to make the half-wave line transformation from valve to load at a ratio compatible with the highest possible voltage at the load position without giving undue rise to corona or ionization discharges. Allowing for variations in normal ambient conditions such as air temperature, humidity and contamination, r.f. peak voltages of about 12 to 14kV were considered practicable.

Valve Operating Conditions and Circuit Constants

The operating conditions of the two valves upon which the further circuit design is based are as follows:

	YD1172	YD1182	
V_a	6	7	kV
I_a	3·4	5·72	A
$-V_g$	460	564	V
$+V_g$	340	436	V
$I_{g\,(\text{on load})}$	0·92	1·5	A
$I_{g\,(\text{off load})}$	1·35	2·2	A
R_{g-f}	500	375	Ω
p_a	4·2	8·6	kW
P_{out}	16·2	31·44	kW
P_{load}	13·5	27	kW
η_a	79·4	78·5	%

The resultant instantaneous values for the peak anode swing are

	YD1172	YD1182	
$V_{a(pk)}$	5·4	6·4	kV

and therefore, if the tank circuit is to be connected between grid and anode,

$V_{g-a(pk)}$	6·2	7·4	kV

With the generator designed for both valve types, and hence for two different sets of operating conditions, the tank circuit capacitor must be so dimensioned that the resultant Q_L values will sustain stable oscillations under industrial conditions with the larger valve (lower anode impedance) and cause no excessive circuit losses with the smaller one (higher anode impedance), that is Q_L should lie between 25 and 50.

From the above figures a transformation ratio of 1:2 can be seen to be satisfactory and since this, together with the load position capacitance, will determine the generator tank capacitance, an assessment must be made to establish whether the resultant loaded Q will satisfy the above mentioned industrial conditions.

If the noted load powers are to be dissipated in a dielectric load, a specific load volume must be considered. The design example load was formed by a number of cylindrical pellets of wood-loaded urea formaldehyde, each having a diameter of 5cm, a height of 3·5cm and weighing 75g.

The material has, at room temperatures, a dielectric constant (ε′/ε) of 5·1, a loss factor (tan δ) of 0·05, and a specific heat (S) of 0·4.

Assuming, in the first instance, no changes of these figures during the process, the weight of load (m) which could be raised in temperature by 100degC with 13·5kW (YD1172) in 15 seconds, can be derived from the equation

$$P_{\mathrm{load}} = \frac{(\theta_2-\theta_1)\times m\times S\times 4{\cdot}2}{t}. \qquad \ldots(8)$$

Therefore,

$$m = \frac{P_{\mathrm{load}}\times t}{(\theta_2-\theta_1)\times S\times 4{\cdot}2} = \frac{13\,500\times 15}{100\times 0{\cdot}4\times 42} = 1210\mathrm{g}. \qquad \ldots(9)$$

As soon as heating starts, the dielectric constant and, to a much larger extent, the loss factor will increase (the latter to about double). The processing conditions can therefore only apply during the power peak of the processing cycle. It is this figure that is the generator rating.

Further calculations were based on the changed loss factor and, assuming that there will also be some thermal losses, showed that 1000g (or 14 test pellets) represent a reasonable test load for the YD1172. For the YD1182 this would be doubled. The capacitive area occupied by these pellets will then be 275cm² and the resultant load capacitance given by

$$C_W = 35\mathrm{pF}$$

and

$$X_C = 150\Omega.$$

For the increased loss factor the potential difference V across the load will be given by,

$$V = \sqrt{\left(\frac{P_{\mathrm{load}}\times X_C}{\tan\,\delta}\right)} = \sqrt{(13\,500\times 150\times 10)}\mathrm{V}$$
$$= 4{\cdot}5\mathrm{kV}_{\mathrm{r.m.s.}} \text{ or } 6{\cdot}3\mathrm{kV}_{\mathrm{pk}} \qquad \ldots(10)$$

By capacitive division the necessary air gap above the load material will then be 7·5mm.

Though load plates made to the above dimensions would be adequate, other practical considerations suggested that their area should be much larger than the calculated values.

1) If the load plates are no larger than the dimensions of the load material, the latter will be subject to the capacitive edge effects of the load plates, and uneven heating will result.
2) Larger area load plates will allow the accommodation of a wider range of load shapes in a general purpose dielectric heater.
3) The total resultant load position capacitance can thus be made considerably larger and thereby used to swamp some of the capacitive changes that take place in the load material during processing. An improved frequency stability of the generator will result.

For these reasons a load plate size of 50×50cm = 2500cm² was considered adequate for a large range of possible pre-heating and process drying applications. The opposing capacitive plate, for reasons similar to those above, must be adjustable. A mean plate spacing of 5cm was assumed in the calculations of the load position capacitance, making this capacitance 44pF. This is sufficiently low to permit the addition of a set of differential capacitive plates that will partially compensate for any capacitive changes caused by different settings of the dielectric gap.

The final load position capacitance was accordingly made

$$C_L = 50\mathrm{pF}.$$

When computing the generator end-capacitance, allowance was made for the fact that capacitors, comparable in their dimensions to the inductive path length of the circuit in which they are mounted, will show a significant voltage decay along their surface in the direction of the r.f. current flow, with the consequence that their effective contribution to the circuit capacitance is smaller than their calculated value would suggest. This effect will increase with increasing capacitance, since, for a given dielectric and frequency, both the physical size as well as the r.f. currents causing the potential decay along the surface will increase, and the inherent inductive component will constitute a larger proportion of the total circuit inductance.

If, then, a line transformer is to be constructed with a transformation ratio larger than one, the ratio of the end loading capacitances must be larger than the theoretical calculation suggests (see Eq. 7), so that instead of

$$T = \frac{C_G\,\cos\,\theta_L}{C_L\,\cos\,\theta_G} \qquad \ldots(11)$$

the empirical relation

$$T' = \sqrt{\frac{C_G}{C_L}} \qquad \ldots(12)$$

more accurately satisfies practical requirements. In the above expressions T and T′ are the transformation ratio, C_G and C_L the end-loading capacitances and cos θ_1 and cos θ_2 the corresponding lengths of the shortened line measured in radians.

With the stated requirement that

$$T' = 1:2$$

the end-loading capacitances need to have a ratio of

$$C_G/C_L = 4.$$

Therefore

$$C_G = 200\mathrm{pF}.$$

This value includes the c_{a-g} (24pF) of the YD1172 and will be only slightly larger (208pF) for the YD1182 for which the c_{a-g} is 32pF.

The resultant Q_L values for the two operating conditions will then be

	YD1172	**YD1182**
Q_L	47	38

Both are acceptable for industrial operation. (These figures ignore the distributed line capacitance which is very small compared with the loading capacitance.)

Line Dimensions

All further line dimensions are mainly determined by the electrical requirements as well as physical size of the end-loading capacitances, including the fact that their major dimensions, in order to exert the maximum capacitive effect on the line, should be at right angles to the line axis. Since the load plate is 50×50cm and one of the end-faces of the line-outer conductor forms the opposing capacitive area, the line-outer was given a cross-sectional area of 70×70cm, allowing for an adequate voltage gap to the edge of the load plate.

The dimensions of the line-inner conductor are then such that the conductor is subject to an amount of undesirable losses that are still acceptable for most applications. Since one of the aims of the present design was the construction of a circuit with minimum losses, the natural line impedance was chosen to be 77Ω as a compromise between line length and losses. For this the ratio of line-outer diameter (D) to line-inner diameter (d) is

$$D/d = 3{\cdot}6.$$

This results in a line-inner cross-section of 19·5×19·5cm. The line length was then calculated by treating the generator section of the line and load section of the line as separate quarter-wave resonators and the following values were found.

Length of generator section	ℓ_G =	40cm
Length of load section	ℓ_L =	130cm
Half-wave length	$\ell\lambda/2$ =	170cm

Some modification of these figures was necessary to account for the physical size of the end-loading capacitances. The load-position capacitive plate is equivalent in its inductive value to about 20cm of the calculated line length, reducing ℓ_L to 110cm. To an even larger extent this argument applies to the generator end capacitance of 200pF, because this value must be accommodated within the given line cross-section whilst maintaining an industrially safe dielectric spacing of 3·5cm. The available capacitive area at the generator end-face of the line is thus only 63×63cm, resulting in a capacitance of 97pF. The remainder was made up by extending the capacitive area, with the same dielectric spacing, parallel to all four sides of the line outer, by 25cm and adding the c_{a-g} of the smaller valve. The capacitance thus obtained would be 188pF, but is reduced to the necessary 103pF through the loss of area caused by a ventilation grille.

The inductive contribution to the line length of this box shaped capacitive extension, together with a 10cm taper between the latter and the 77Ω line inner, is approximately equivalent to 60% of the previously calculated generator line length of 40cm so that the total overall line length is:

Load line section:	130cm
Equivalent inductive length of load plate:	−20cm
Calculated generator line section:	40cm
Taper:	10cm
Capacitive box depth:	25cm
Equivalent inductive length of taper and capacitive box:	−25cm
Total length of λ/2 line inner:	160cm

An undesirable concomitant of the abrupt dimensional changes from the 77Ω line inner to the capacitive box, as well as the relatively great length of the box in comparison with the originally calculated generator section line length, is the creation of a secondary resonance. However, since its origin is known measures to render this resonance ineffective, as far as the oscillatory functions of the valve are concerned, are fairly simple (see page 144).

DETAILS OF OSCILLATORY CIRCUIT

For the oscillatory functions, only the generator section of the half-wave line need be considered. With the anode connected to the line-outer and the grid to the line-inner, as shown in Fig. 5, the effective tank circuit appears between grid and anode, and the basic configuration for a common grid oscillator is established.

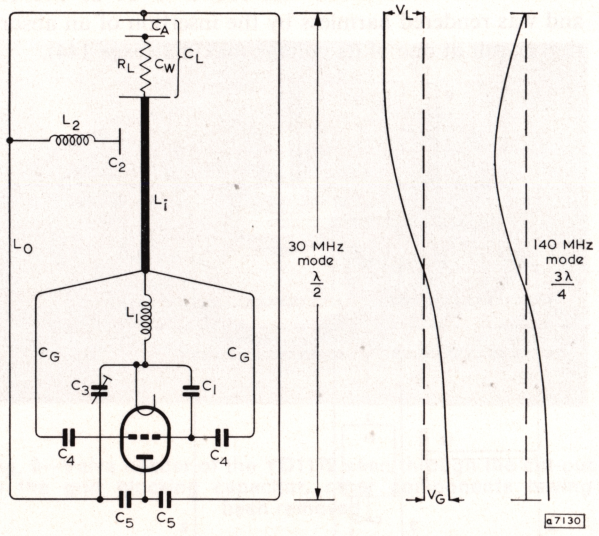

Fig. 5—Basic circuit of a half-wave line dielectric heater, not to scale. The components are as follows: R_L, resistance of load material; C_W, capacitance of load material; C_L load position capacitor 50pF; C_G, generator tank circuit capacitor 200pF; C_1 drive circuit loading capacitor 140pF; C_3 ,feedback capacitor 2 to 20pF; C_4, grid blocking capacitor, 2·5nF (p.t.f.e. sandwich); C_5, anode blocking capacitor 1·5nF (p.t.f.e. sandwich); L_i, 77Ω line section; L_O, line outer case; L_1, drive circuit inductor. The components L_2 and C_2 are for absorbing a secondary mode at 140MHz and are described in the text on page 144

The necessary ‘drive circuit’ reactance between grid and cathode is furnished by a tuned circuit of relatively high C/L ratio assisting in the suppression of higher frequency modes or harmonics. The resonance frequency of this circuit is moreover set about 40% below that of the tank circuit to make the feedback conditions less dependent on the frequency changes that may occur in the tank circuit, especially with varying settings of the dielectric gap of the load position. For the nominal tank circuit frequency of 30MHz this drive circuit was tuned to 18MHz. Although this setting is in no way critical, care was taken to avoid any of the sub-harmonics of the oscillator as these might increase the harmonic content in the anode waveform.

The feedback system for a common grid-tuned anode-tuned cathode circuit as described above is provided by the addition of external cathode-anode capacitance, the amount being governed by the feedback ratio of the valve. The appropriate values of capacitance for the two valves operated under the conditions given on page 137, are then,

	YD1172	**YD1182**	
$C_{feedback}$	5·7	9·4	pF

Because of the r.f. voltage losses that are to be expected in the feedback structure, these values will in practice be somewhat higher, and are adjusted with the help of a variable capacitive component. Practical useful limits of this capacitive variation lie between −20% and +50% of the design value. This precaution, if necessary, also caters for operating conditions other than those specified.

In addition to the basic half-wave circuit Fig. 5 also shows the approximate r.f. potential distribution at the fundamental frequency as well as the high frequency mode generated by the tank circuit capacitive box. The resonance of this latter mode was found to be at 140MHz and was rendered harmless by the insertion of an absorption circuit at one of its voltage maxima (page 144).

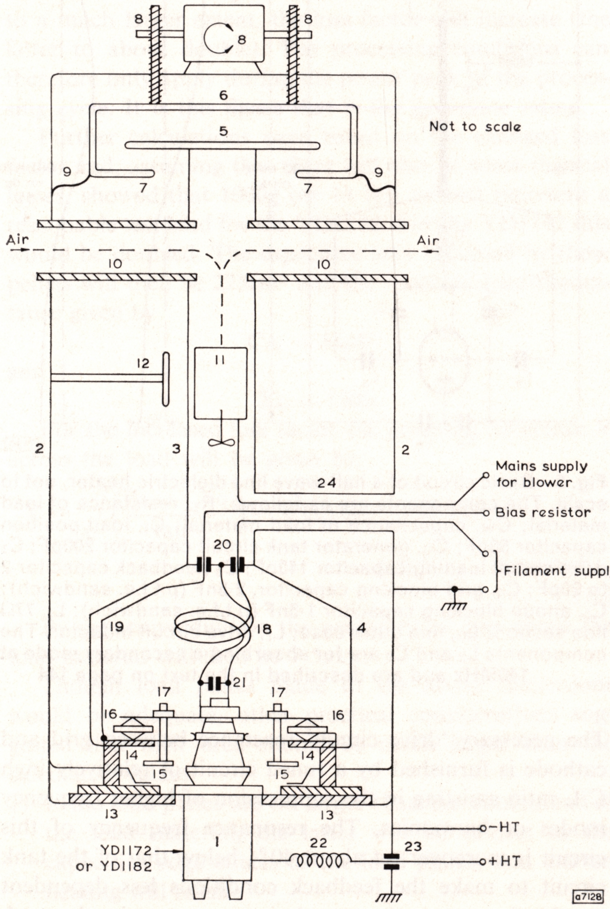

Fig. 6—Sectional sketch of half-wave dielectric heater. Components are as follows: (1) valve (2) line-outer (3) 77Ω line-inner (4) generator tank capacitor box (5) lower load capacitive plate (6) upper load capacitive plate (7) differential capacitor plates (8) motor and gears for load setting (9) copper foil straps (10) air ducts (11) coaxial blower (12) 140MHz mode suppressor circuit (13) anode blocking capacitor (14) grid blocking capacitor (15) feedback capacitor (16) drive circuit loading capacitors (17) collets for feedback adjustment (18) drive circuit inductor and filament supply (19) grid bias lead (20) bias and filament decoupling (21) filament decoupling capacitor (22) h.t. filtering choke (23) h.t. filtering capacitor (24) feed-through tube

Circuit Layout

The practical layout of the half-wave dielectric heater follows essentially the outlines suggested by the basic circuit of Fig. 5 and is shown in more detail in Fig. 6 where blocking capacitors, feed lines etc. are included.

The line-outer, which is also the main supporting structure, forms a prismatic box of 70×70×195cm; the extra height contains the motorised load matching mechanism. The structure is shown in Fig. 7.

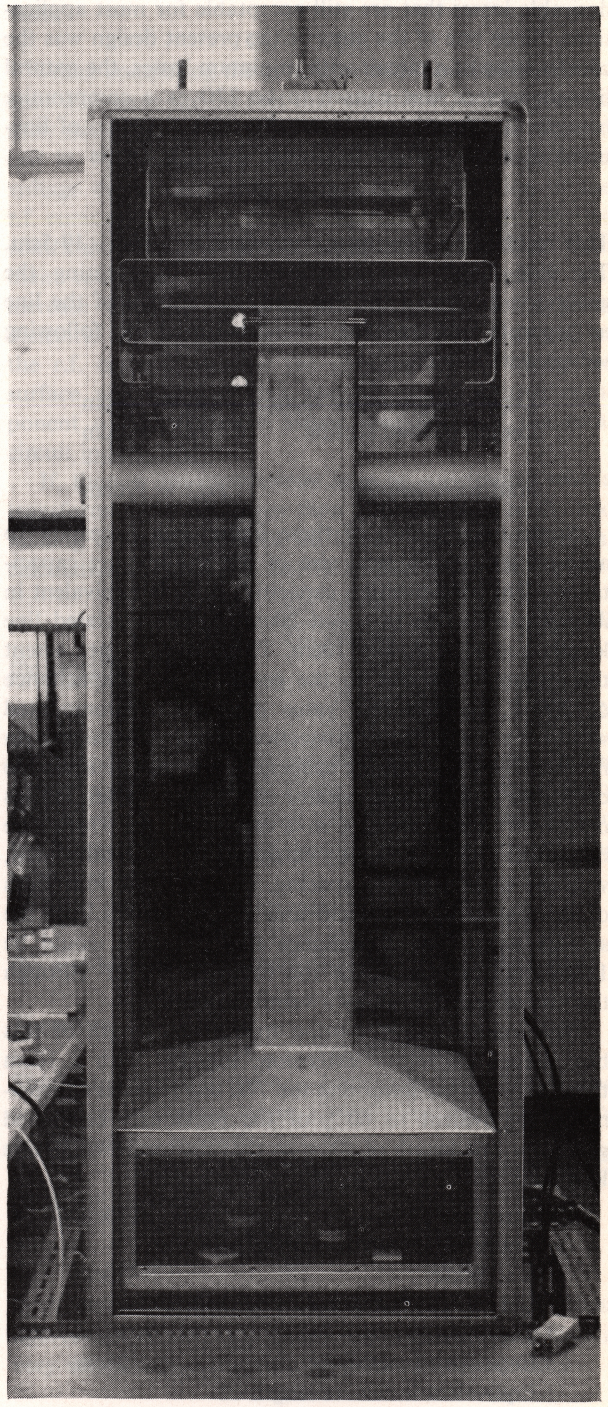

Fig. 7—Overall view of 30MHz half-wave line dielectric heater, with the front panels of the line-outer and the tank circuit capacitor box removed

The valve anode blocking capacitor, a p.t.f.e. sandwich with 1·5nF capacitance, is mounted at the bottom end-face of the line-outer. The valve, being supported at this level by its mounting flange, protrudes with the bulk of its anode structure and cooling system below the line box. Since the outer surface of the anode is thus outside the r.f. field of the line, the water hose coil, visible in Fig. 8, need be dimensioned to cope only with the d.c. supply voltage drop. A further capacitive plate of the same dimensions as the blocking capacitor is electrically connected with, and placed parallel to, the blocking capacitor so that the dielectric spacing between anode and grid level will be 3·5cm. This can be seen in Fig. 9.

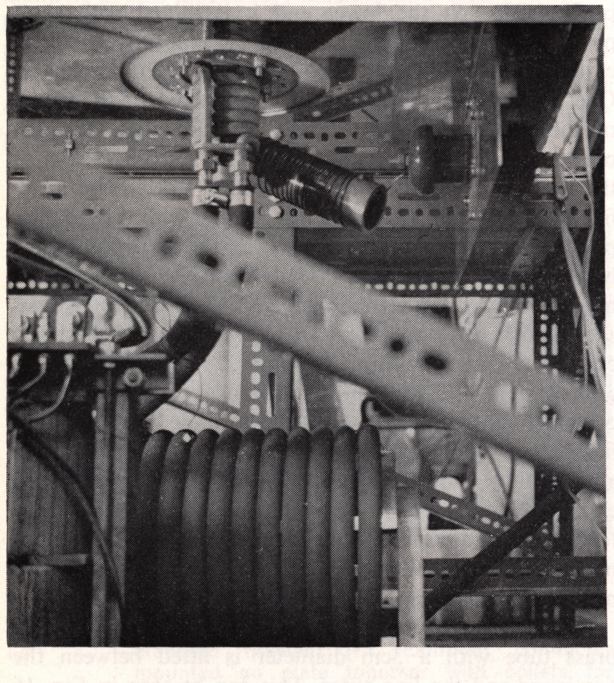

Fig. 8—Underside of line structure of prototype heater with YD1172 cooling helix protruding. To the right of the anode are the anode supply filtering choke and capacitor. The drum for the anode cooling-water hose can be seen beneath the anode

The line-inner, consisting of the tank circuit capacitor box and the 77Ω line section and loading plate, is supported by the bottom face of the tank capacitor box, at the level of the grid ring of the valve, by four polypropylene pillars (Fig. 10). Its lateral positioning is secured by two 10cm diameter polypropylene tubes between two opposing vertical panels of the line outer, 25cm from the top end of the line. These supporting tubes serve at the same time as air intake ducts for the fan that is mounted inside the line-inner and used to provide the necessary forced air cooling for the valve header.

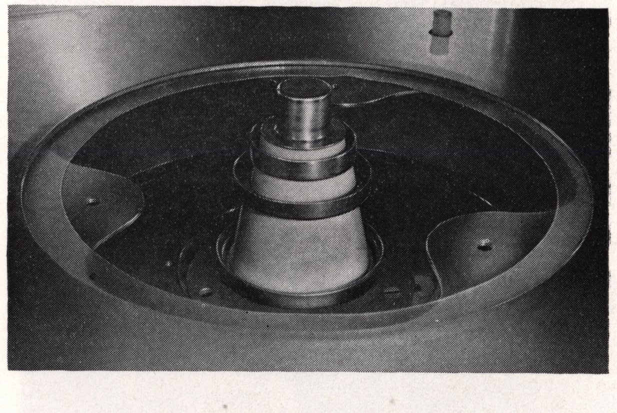

Fig. 9—Valve header of the YD1172 seen through the cut-out in the grid blocking capacitor, other components having been removed

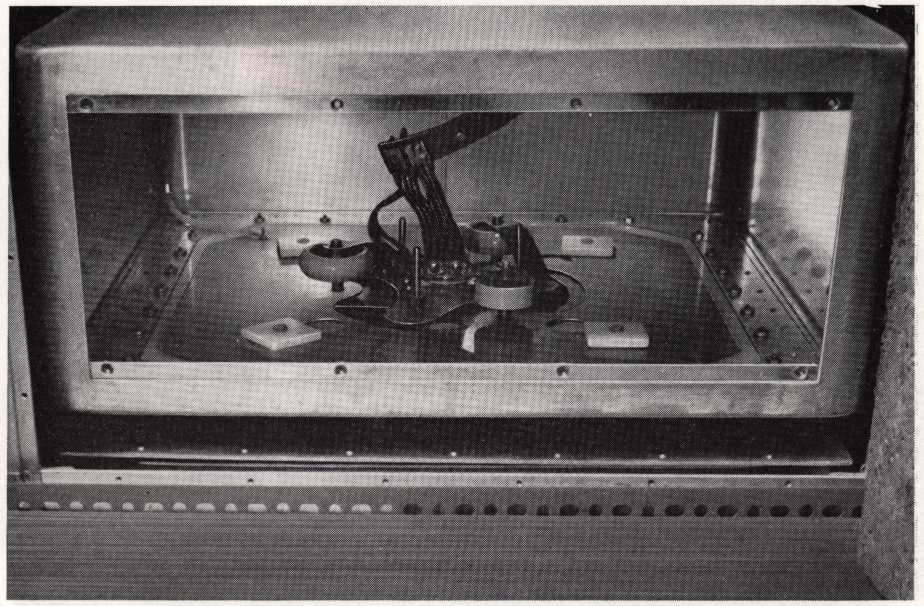

Fig. 10—Tank circuit capacitor box, containing the grid-filament circuit. The large p.t.f.e. sandwich capacitor at the bottom of the box is the grid blocking capacitor. The grid bias lead is connected at the rear left-hand corner and is dressed along the inside of the box for decoupling purposes

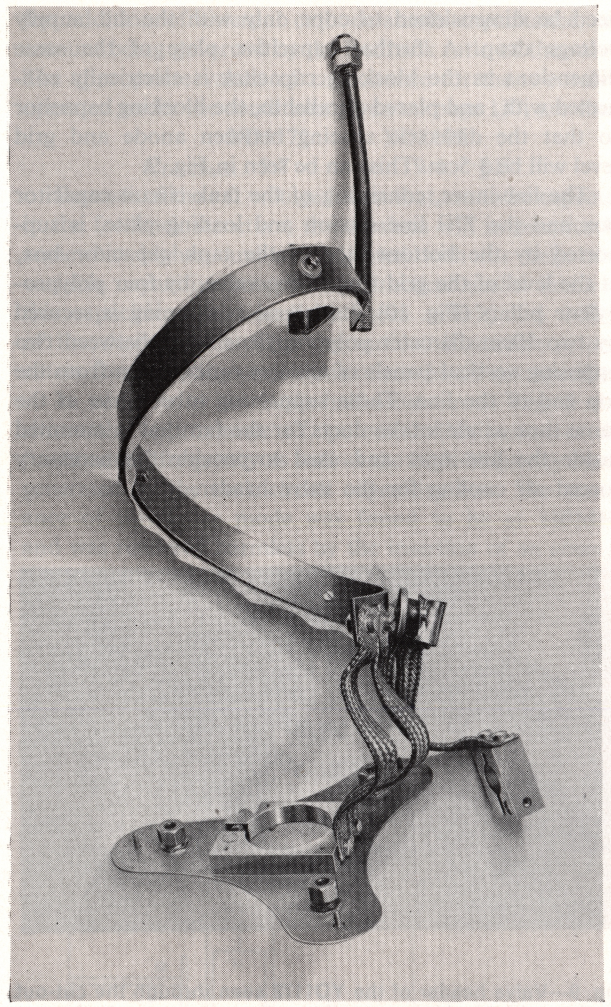

Fig. 11—Grid-cathode circuit inductor with filament connectors

The inside of the tank circuit capacitor box contains the grid-filament circuit and is connected through the grid blocking capacitor and a finger strip grid connector to the grid of the valve. Fig. 11 shows a $1\frac{1}{2}$ turn coil of 17cm diameter which serves the dual purpose of drive circuit inductor and filament supply leads. It is manufactured from two 55cm copper bars, of cross-section 5×25mm, wound in parallel and interleaved with 0·5mm thick p.t.f.e. strip. At the lower end it is joined with short pieces of flexible copper braid to the respective filament connectors (Fig. 12) and decoupled with a 2nF capacitor. One of the upper limbs of this coil is fixed to the centre of the top of the tank circuit capacitor box and the other with a feed-through capacitor to the inside of the lower part of the 77Ω line section inner. The lower filament connector (r.f. cathode) is fitted with a triangular plate, similar to that of the grid connector, but off-set by 60°, and carries on its upper surface three collets holding the C_{a-f} feedback capacitor. Between the underside of this plate and the grid blocking p.t.f.e. sandwich capacitor, there are three ceramic capacitors serving as grid-cathode circuit loading capacitances with a total value of 140pF. Into the collets on the cathode connector are fitted three 6·5mm rods which reach downwards through gaps in the grid blocking capacitor and carry a ring shaped electrode facing the anode blocking capacitor, thereby forming the adjustable feedback capacitor. These components are shown in Fig. 13 and their approximate relative positions are shown in Figs. 14 and 15.

Near the zero voltage point on the 77Ω line-inner, a brass tube with a 3cm diameter is fitted between the line-inner and the line-outer. This can be seen in Fig. 16 and it fulfils several functions: firstly, it serves as a d.c. ground connection to the line-inner; secondly, it carries one limb of the valve filament current; finally, it screens from r.f. the other filament limb as well as the grid bias lead and the mains supply leads to the blower motor (mounted inside the line-inner). At first sight, it might appear that this brass tube would tie the line-inner to the line-outer as far as their respective r.f. functions are concerned, and thereby split the half-wave line into two quarter-wave circuits, losing the advantage of the floating zero voltage point. This is not so, however, since the diameter of this tube is very much smaller than that of the line-inner and will therefore represent a relatively high impedance in parallel with the much lower one of the 77Ω line-inner. Its resultant effect on the position of the zero voltage point, the operational frequency and the transformation ratio is negligible.

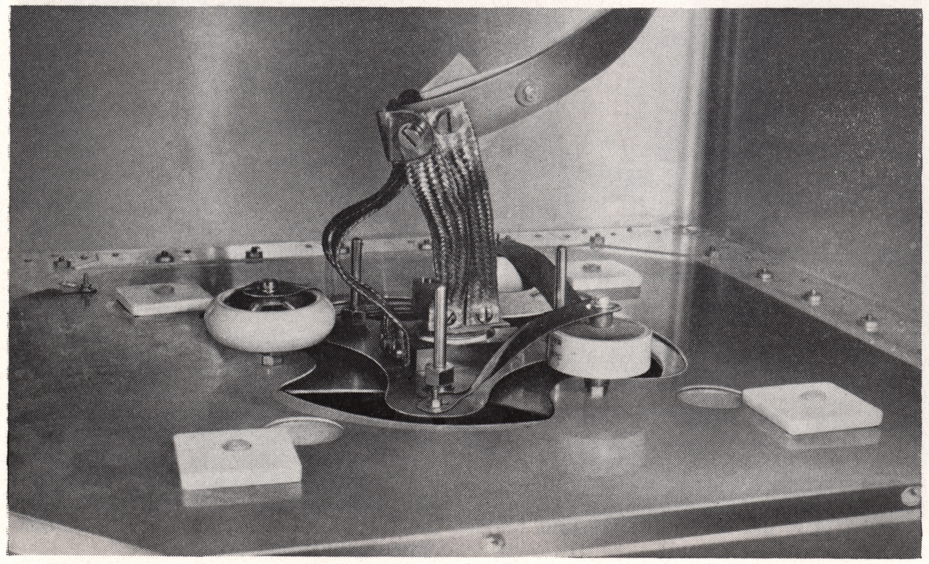

Fig. 12—Grid-cathode circuit and feedback assembly. Three ceramic capacitors (total 140 pF) are grouped round the valve header and connected between filament (cathode) and grid plates. The three adjustable rods, holding the feedback ring, can be seen protruding from the collets on the filament (cathode) plate

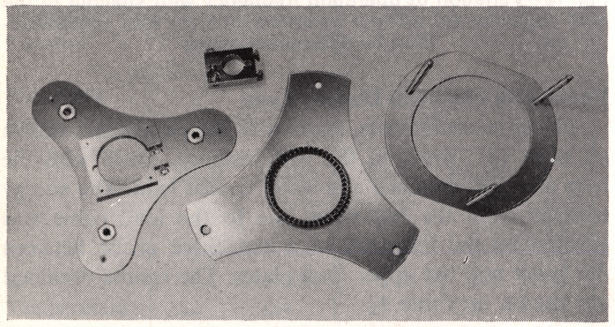

Fig. 13—Components used in connecting the valve
Top centre—standard filament connector
Left —standard filament (r.f. cathode) connector mounted on plate together with collets for feedback ring
Centre —grid-connector manufactured from brass plate and phosphor-bronze finger-strip
Right —feedback ring with mounting rods

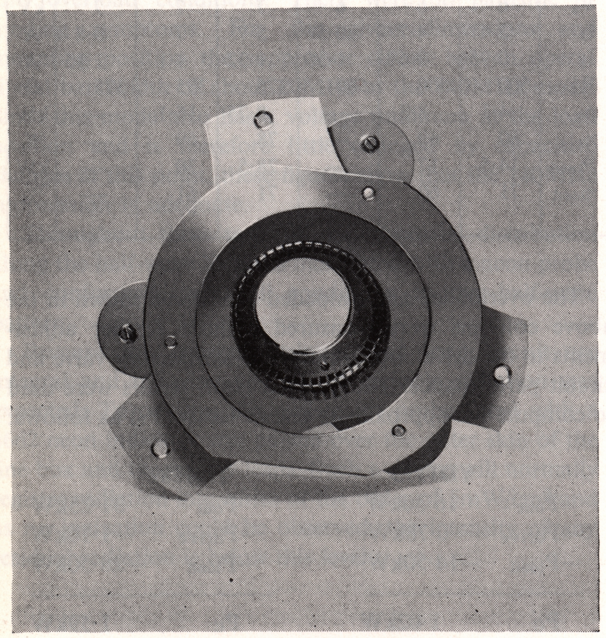

Fig. 14—End-on view of components shown in Fig. 13, assembled in approximately their correct relationship

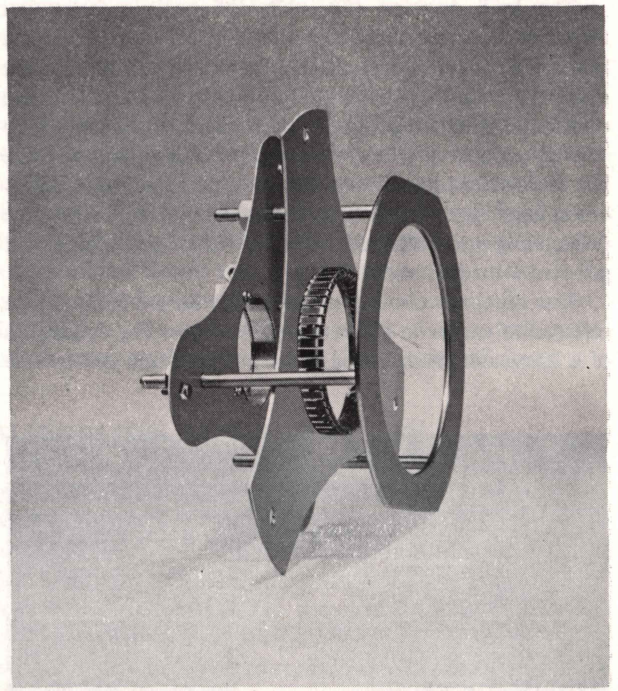

Fig. 15—Side view of components shown in Fig. 13, assembled in approximately their correct relationship

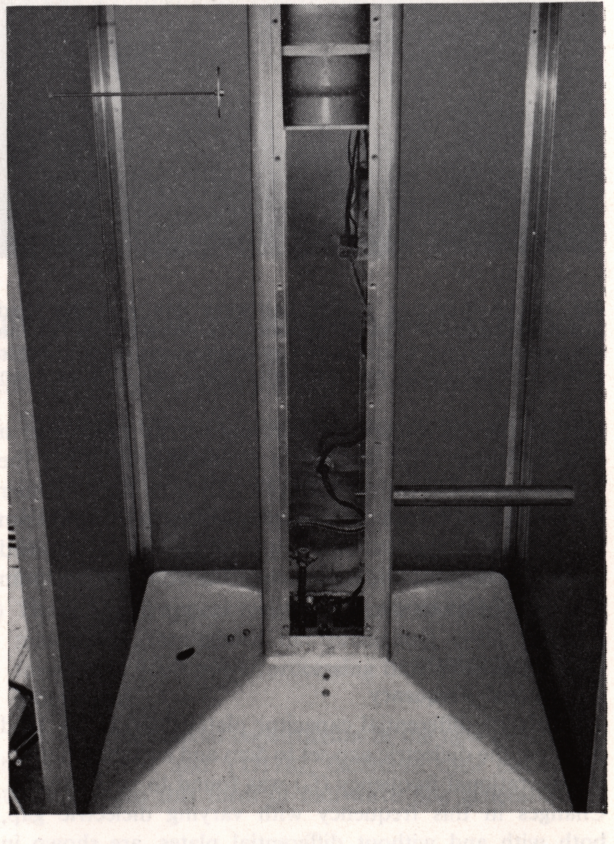

Fig. 16—Generator section of line, and tank capacitor box. The 140MHz mode absorption circuit can be seen at the top left, and the tube between the line-inner and outer can be seen at the bottom right. The tube carries supply cables for the filament, the grid bias, and mains for the coaxial air blower. Part of the blower is visible at the top, inside the line-inner

The load position (Fig. 17) differs little from that found in a conventional dielectric heater. It consists of a horizontal 50×50cm loading plate at the top end of the line-inner together with the opposing capacitive plate connected with copper foil straps to the line-outer. Two smaller capacitive plates connected to this opposing plate but facing the underside of the load plate act as a differential capacitor, minimising the frequency shift when the dielectric gap is adjusted with the aid of the motor and gear train located above.

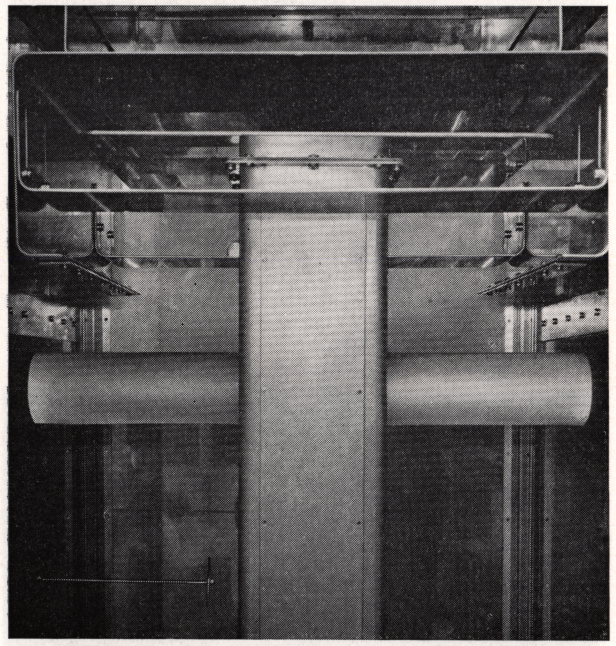

Fig. 17—Load-section of the half-wave line with the load position capacitor. The differential capacitive plates can be seen to be preset adjustable in relation to the main variable plate. The horizontal polypropylene tubes can also be seen

The acceptor circuit, suppressing the 140MHz mode referred to earlier in the text and shown in Fig. 5, consists of a 22cm×4mm threaded rod fixed with one end to one side of the line-outer and carrying on its other end a capacitive disc. This disc has a diameter of 6cm for the YD1172 and 8cm for the YD1182, and faces the line-inner at a distance of 4cm. Its vertical position is 110cm from the bottom of the line and this position was determined by the location of the most accessible voltage maximum of the 140MHz mode.

PERFORMANCE

Operational Frequency

With the differential capacitor plates fitted at the load position, the dielectric gap set to 5cm and no load inserted, the operational frequency (f_o) was found to be 31·4MHz. Changes in this frequency with varying dielectric gap, both with and without differential plates, are shown in Fig. 18, where it can be seen that the stabilisation of frequency with the help of the differential plates is considerable. They were therefore used in all the measurements noted.

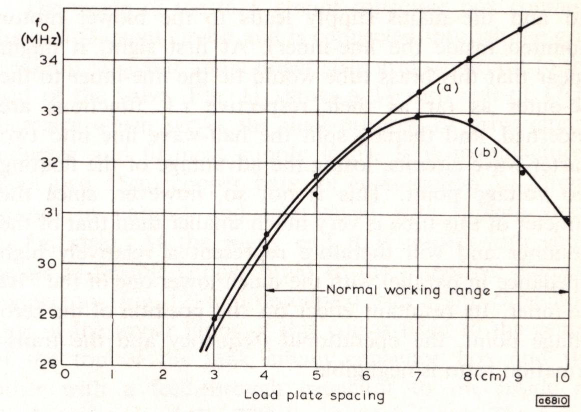

Fig. 18—Variation of operating frequency with spacing of the load capacitor (a) without compensation (b) with compensation by differential plates

Power with Electrical Dummy Load

Power measurements, made with the parameters shown on page 137, were, in the first instance, made with the help of a 50Ω matched and water cooled load. The energy transfer from the half-wave line to the load cable was effected by the insertion of a capacitive probe between the lower and the upper load plates. The results obtained are shown in Table 1.

TABLE 1

Performance of YD1172 and YD1182 in Half-wave Dielectric Heater

	YD1172			YD1182			
	Normal load	Over-load	Off load	Normal load	Over-load	Off load	
V_a	6	6	6	7	7	7	kV
I_a	3·4	4·7	0·54	5·7	7	0·8	A
I_g	0·95	0·67	1·36	1·32	1·1	1·85	A
R_g	500	500	500	375	375	375	Ω
p_a	4·1	8·8	—	8·75	15·1	—	kW
η_a	80	69	—	78	69	—	%
P_{load}	14·5	17	—	28·5	30	—	kW
η_{load}	71	60	—	71	61	—	%

The overloaded and unloaded conditions shown in the above columns were measured without further adjustments to the drive circuit and show satisfactory valve and circuit performance. The 'normal load' results were used to compute the approximate circuit losses (P_c) as follows:

YD1172		YD1182	
P_{out}	16·30kW	P_{out}	31·25kW
$-P_{drive}$	−0·78kW	$-P_{drive}$	−1·16kW
$-P_{load}$	−14·50kW	$-P_{load}$	−28·50kW
P_C	1·02kW	P_C	1·59kW

These give the corresponding circuit transfer efficiency figures (η_C) below.

(YD1172) $\eta_C = 94\%$ (YD1182) $\eta_C = 97\%$

Performance with Practical Load

For practical operation, the design example material of wood-loaded urea formaldehyde pellets was used. Press moulding technology requires that the temperature of this type of material should rise by a minimum of 100degC in less than 45s of pre-heating. Table 2 gives sets of figures for the start and finish of the process.

TABLE 2

Performance of Prototype Dielectric Heater

	YD1172		YD1182		
Weight of material	1		2		kg
Processing time	15		15		s
	Start	Finish	Start	Finish	
V_a	6	5·8	6	5·6	kV
I_a	2·8	3·6	5·2	6·1	A
I_g	1·1	0·91	1·28	1·1	A
Temperature	22	124	22	125	°C
f_o	31·0	30·7	31·6	31·0	MHz
Maximum deviation of f_o during process	−300		−600		kHz

To check both the operational stability of the oscillator and the functioning of the 140MHz-mode suppression, switching tests were carried out under off-load, full-load and overload conditions. There were no parasitic or moding symptoms. For the given dimensions and mounting position the suppressor circuit has an operational bandwidth of about 20MHz at the 140MHz mode. Since this mode also has a voltage minimum at the load position and is therefore little changed by capacitive changes at this point, these figures show that the 140MHz suppression is adequate.

Throughout these tests the r.f. potential distribution along the half-wave line was monitored with a neon probe and conformed under all conditions to the half-wave pattern.

Because the generator circuit and load circuit are integral and self screening, no appreciable radiation was expected. To confirm this a detector probe fitted with a 4662 neon indicator was passed over the outer skin of the line box and the supply leads. Such a device will normally register radiation intensities of the order of 5mW/cm² and as no ionisation could be observed, the intensity of any residual radiation is below this level.

Circuit Losses

Though the off-load currents noted in Table 1 may seem large for a 'minimum loss' design the following circumstances must be taken into account. The circuit losses of the half-wave line generator can, in the first approximation, be assumed to be double that of a corresponding quarter-wave line generator in the off-load condition. This is because the coupling of the load circuit to the quarter-wave line generator is very much reduced by the action of removing the load, eliminating most of the losses in the secondary circuit. Under full load conditions, however, and assuming a correct match of the separate load circuit into a quarter-wave generator, both systems will dissipate the same amount of circuit losses. The higher off-load current apparent with a half-wave circuit does not therefore reduce the transfer efficiency.

ALTERNATIVE TANK CAPACITORS

Reductions of the overall dimensions of this type of generator could be achieved if suitable ceramic capacitors were available for the generator tank capacitance. Two further operational advantages would then also accrue. Since the reduction in dimensions would substantially reduce the present vertical dimension of the generator tank capacitor box, the secondary mode (now at 140MHz) would be eliminated by being shifted well into the transit-time region of the valve. Secondly, the generator tank capacitance could be increased and hence the stability at the operating frequency be improved, without substantially adding to the vertical line dimensions. In the same way a further reduction of the line length would be obtained if both line end capacitors were increased proportionately with the same transformation ratio.

ALTERNATIVE CIRCUIT DISPOSITIONS

There are no reasons why the present grid-anode connection relative to the line should not be reversed or the location of generator and load section be reversed if a specific application makes this desirable.

ADVANTAGES OF HALF-WAVE LINE HEATER

The advantages of the half-wave line over more conventional circuits can be summarised as follows:

1) The construction of a half-wave generator-load circuit is extremely simple as it differs very little in its physical layout from the theoretical circuit diagram.
2) High r.f. potentials may be obtained by line transformation without the introduction of additional reactances that normally cause parasitic oscillations.
3) The load will appear resistive because unity coupling is maintained throughout the processing cycle, and a favourable 'load power/processing time' relationship is maintained.

The ceramic coaxial construction of the new industrial triodes, YD1172 and YD1182, facilitates their electrical integration into this form of half-wave line generator.

COMPONENTS FOR PROTOTYPE

It should be noted that Mullard Ltd do not make or supply any of the constructional components used in this prototype heater, except the valves YD1172 and YD1182.

A 400kHz Induction Heater of Advanced Design for Powers up to 60kW

D. E. NIGHTINGALE
Mullard Central Application Laboratory

An improved form of high power induction heater, operating at 400kHz, has been designed without chokes and anti-parasitic devices. The r.f. circuit elements are used to feed the d.c. potentials to the generator valve terminals. High load efficiencies and complete freedom from parasitic oscillations have been obtained even at severe overloads.

The oscillator has operated satisfactorily at output powers up to 60kW with three of the new range of ceramic envelope industrial triodes, namely the YD1172, YD1182 and YD1192.

INTRODUCTION

Experience of high power industrial heating generators over the years has shown that instability in the generator can often be attributed to parasitic resonances. The presence of parasitic oscillations has tended to be accepted both in normal operation and in fault conditions and the use of anti-parasitic devices which are palliatives has become widespread. This article is intended to show that by careful circuit design and construction such parasitic oscillations can be avoided under all operating conditions including severe overloads.

An oscillator (Fig. 1), designed with these principles in mind, has been constructed to show the performance of the ceramic envelope industrial triode valves type YD1172, YD1182 and YD1192 in such a generator.

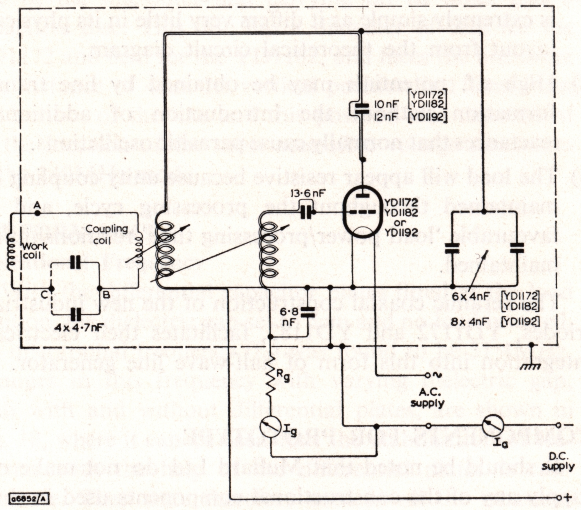

Fig. 1—Circuit of induction heater oscillator

DESIGN CONSIDERATIONS

Instability in generators can usually be attributed to one or more of the following:

1) resonance of the h.t. feed choke with associated capacitances
2) resonance of the grid feed choke and blocking capacitor and by-pass capacitor
3) resonance of filament capacitors and chokes when used
4) inductive interconnections between components, including the valve
5) chassis currents giving rise to unwanted coupling.

Filtering Arrangements

The LC filtering arrangements for the supply lines to the valve can cause parasitic circuits to be set up by virtue of their own self resonances, due to physical size and disposition relative to other components. Damping arrangements and parasitic stoppers can give rise to further instability by causing further unwanted circuit resonances. If the normal LC arrangement can be dispensed with, these problems can be avoided and component costs may be reduced.

Intercomponent Connections

Although the frequency of operation is only of the order of hundreds of kHz, to reduce unwanted coupling, undesirable phase shift effects and r.f. voltage drop, it is necessary that intercomponent connections be kept as short and of as low inductance as possible. The result of this careful design is the elimination, at source, of any potential parasitic resonances due to lead inductance.

Chassis Currents

Chassis currents can cause undesirable feedback effects and should be avoided as far as possible for the following reasons:

1) unwanted coupling due to more than one current following a common path
2) unwanted coupling due to components on or near the chassis
3) power loss in the chassis.

These effects have been avoided in the present design by using only one common earth return to the oscillator.

The use, and the disadvantage, of the usual filter system in the anode d.c. supply has been avoided by passing the supply cable down the inside of the copper tube forming the anode inductor.

TANK CIRCUIT CALCULATIONS

To calculate the tank circuit components the following figures for normal operation are required:

	YD1172	YD1182	YD1192
V_a	6·0	7·5	8·0 kV
$V_{a(pk)}$	5·4	6·8	7·1 kV
$V_{a(r.m.s.)}$	3·82	4·8	5·05 kV
P_{out}	16·25	32·4	63·0 kW

To minimise frequency drift and to ensure reasonable stability without excessive circuit loss a loaded circuit Q of approximately 50 is desirable.

If X_C is the tank circuit capacitance reactance, then:

$$X_C = \frac{V_{a(r.m.s.)}{}^2}{Q_L \times P_{out}},$$

so for each valve:

$$\begin{array}{lccc} & \text{YD1172} & \text{YD1182} & \text{YD1192} \\ X_C = & \dfrac{3{\cdot}82^2\times10^6}{50\times16{\cdot}2\times10^3}\Omega & \dfrac{4{\cdot}8^2\times10^6}{50\times32{\cdot}4\times10^3}\Omega & \dfrac{5{\cdot}03^2\times10^6}{50\times63\times10^3}\Omega \\ = & 18{\cdot}0\Omega & 14{\cdot}2\Omega & 8{\cdot}03\Omega \end{array}$$

Therefore, C at 400kHz

$$\begin{array}{lccc} = & 22{\cdot}2\text{nF} & 28{\cdot}2\text{nF} & 50\text{nF} \end{array}$$

To operate the three valves without changing the tank circuit inductance, and accepting a lower Q_L for the highest power valve (YD1192), the tank coil inductance was fixed at 6·5μH. The capacitance values were then chosen as follows:

	YD1172	YD1182	YD1192
	24nF	24nF	32nF
giving Q_L values of:	58	46	34

The capacitors had to be chosen from a standard range and, to keep the volume low and interconnections as short as possible and to meet the ratings required, capacitors type T.C.C. HLC 4150 of 4nF each were decided upon to build up the required tank capacitance. It was felt that the resulting small change of frequency from the design frequency of 400kHz was not important and that the circuit losses when the YD1192 was used would be reduced because of the lower relative circulating current.

CONSTRUCTION

The oscillator was assembled inside an aluminium cabinet 1·0m high × 1·4m long × 1·1m deep (Fig. 2). The filament transformer and grid resistor were mounted underneath. The work coil was also mounted outside the cabinet as it would be in practice (Fig. 3). The framework and panels were designed to fit together with well butting joints tightly bolted to minimise losses due to any induced currents.

The tank coil was formed from three 13mm diameter copper tubes brazed together side by side at 150mm intervals (Fig. 4). The coil internal diameter was 480mm and the total length was 355mm made up by evenly spacing 3·75 turns of the three tube assembly. The coil was secured in place with Paxolin clamps.

The earthy end of the tank coil was clamped to a copper plate 305mm×690mm×2mm thick carrying the tank capacitors. The other end was clamped to a low inductance copper strap connecting together the live ends of the tank capacitors and also one end of the anode blocking capacitor. The maximum tank circulating current (425A) requires that the coil be cooled. Water for this purpose was passed along one outer tube and back through the other, both input and output being at the earthy end of the coil. The centre tube carries the d.c. supply cable to the anode. The cable, fed in at the earthy end of the coil, emerged at the live end and was dressed so as to lie across the blocking capacitor and thence to the valve anode.

The copper strap connecting the live ends of the tank capacitors to the tank coil was cooled also by the tank coil cooling water by means of a pipe soldered to the strap. This assists the cooling of the capacitors.

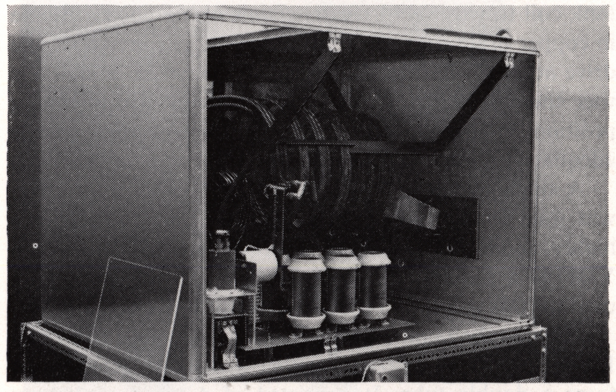

Fig. 2—General view of the equipment. The work coil and load are not visible as they are mounted outside on the right-hand panel

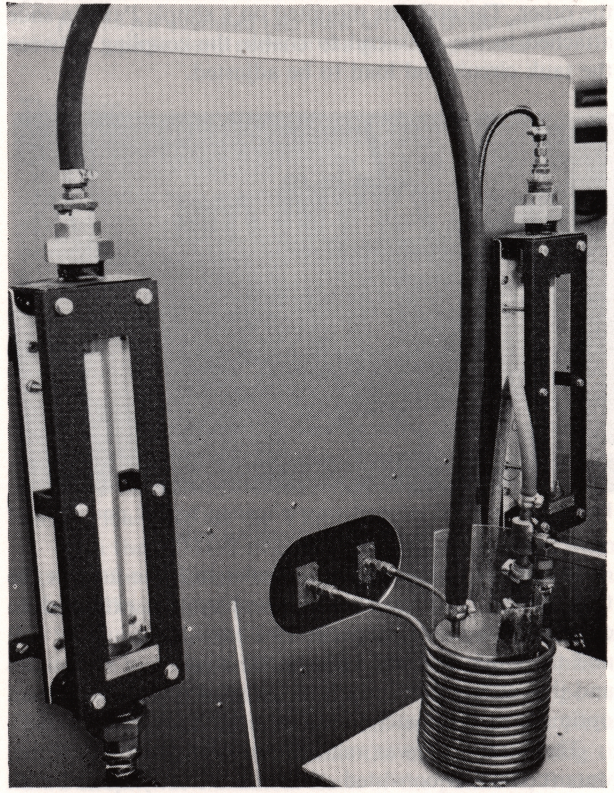

Fig. 3—View showing work coil and water cooled load can with mica insulation to prevent shorting of the coil. The flow meters and thermometers used in some of the measurements are also shown

The tank capacitors were mounted closely together on the copper plate connected to the earthy end of the tank coil. The plate was supported 50mm above the chassis by insulators and bonded to it at the valve end (Figs. 2 and 6).

Considerations of valve-to-circuit connection suggested that the valve be mounted anode upwards. This gives short anode and cathode connections and has the advantage of keeping the anode, with its high potential, clear of the cabinet (Fig. 5).

The grid coil, consisting of 7 turns of 190mm internal diameter, was constructed from a single tube of 6mm diameter with the connection from the grid terminal to the grid resistor running down the centre of the tube. The coil, 90mm long, was wound on a simple insulating framework mounted so that it could be moved relative to the tank coil to vary the drive. The ends of the coil terminate in copper braid to provide the flexibility required to make drive adjustments. Requirement for a separate grid choke was thereby eliminated. The dimensions and coupling position were determined by experiment to provide adequate adjustment of drive for all three valve types.

A single blocking capacitor of 10nF, T.C.C. type 1052, was used for the YD1172 and YD1182. Because of the higher anode potential and increased r.f. current of the YD1192 a bank of three higher voltage capacitors was used for this valve, mounted vertically one above the other.

The coupling coil (Fig. 4) was manufactured from two 13mm tubes spot brazed together at 150mm intervals to form a double tube. It consisted of 4 turns of 380mm internal diameter spaced to give a total length of 200mm. Cooling water was passed along one tube and back through the other. The coil was mounted on a simple Paxolin slide attached to the tank coil to enable the coupling between the tank circuit and load to be adjusted.

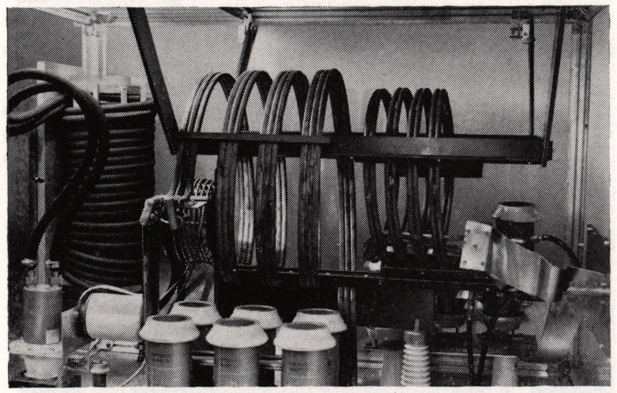

Fig. 4—A detailed internal view showing typical positions of grid, tank and coupling coils

A bank of 4nF capacitors, similar to those used in the tank circuit, and variable in number, was provided to complete the series connection between the coupling coil and the work coil. By varying the number of capacitors and the relative position of the coupling and tank coils an optimum power match could be achieved.

The work coil was made from a single 10mm tube, water cooled. It consisted of 12 turns closely spaced with an internal diameter of 120mm (Fig. 3).

It was desired that the test load should simulate a typical eddy current heated work piece and that the load power should be measured at the same time. To this end a closed can made from 1·5mm steel sheet was used as the load, provision being made to pass cooling water through the can and to measure both the rate of flow and the temperature rise. The can was tightly coupled to the work coil and the power dissipated in the can by induced eddy currents was transferred to the cooling water. The can measured 150mm high × 115mm diameter (Fig. 3).

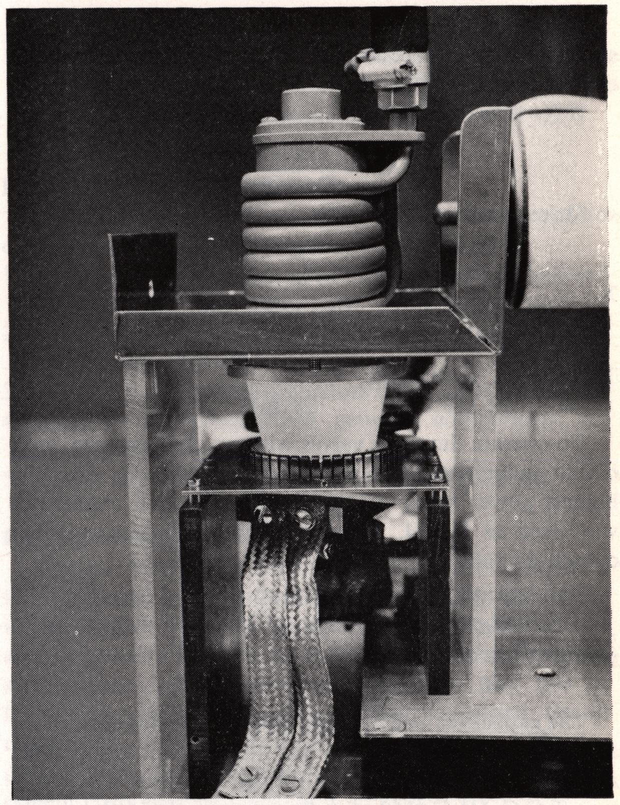

Fig. 5—The YD1172 mounted in the cabinet

MEASUREMENTS

The water flow was arranged in three separate circuits enabling the sources of power loss to be separately determined, namely: anode loss, load power, and the tank coil, coupling coil and work coil losses taken together as a single unit. Thus anode dissipation, load power and circuit losses can all be calculated independently (allowance being made for drive power and filament heating in the temperature rise of the anode cooling water).

The water flow rates in litres per minute were as follows:

	YD1172	YD1182	YD1192
Anode	7·15	7·15	14·3
Load	7·15	14·3	19·0 approx.
Coils	2·4	7·15	3·6

For most tests the water flow was chosen to simplify the calculation of power dissipation. (The coil water flow for the YD1182 could be halved.)

In each water circuit a single thermometer was placed in the outlet side and was used to measure initial and final temperatures, the former being checked before and after heating. Test results are shown in Table 1 (p. 149).

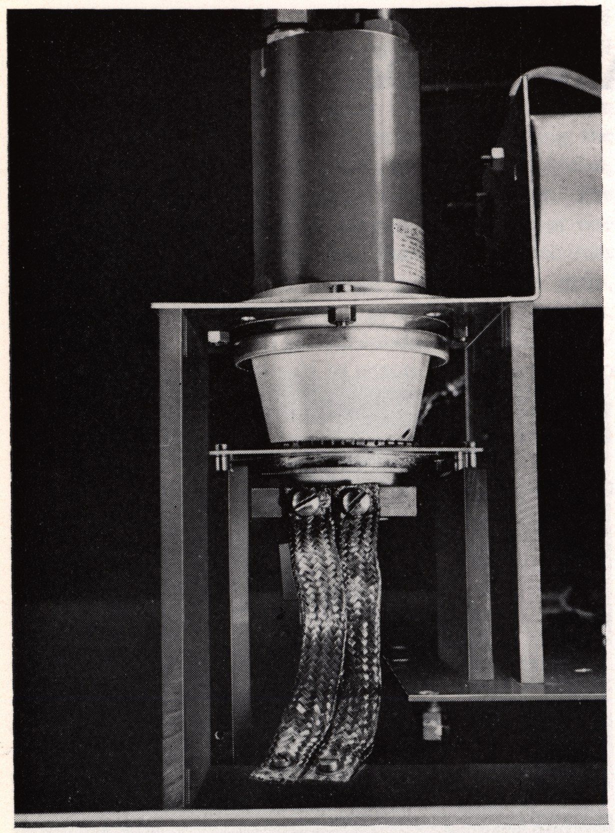

Fig. 6—The YD1182 mounted in the cabinet. The earthing bolt connecting the tank capacitor plate to the chassis is visible at the bottom centre

TABLE 1

Results Obtained When the Operating Conditions Were Set for the Three Valves from the Published Data

	YD1172	YD1182		YD1192	
V_a	6·0	7·0	7·5	8·0	kV
I_a	3·4	5·72	5·4	10·0	A
$I_{g(loaded)}$	0·91	1·46	1·41	2·3	A
$I_{g(off\ load)}$	1·36	2·4	2·23	3·5	A
R_g	500	375	450	300	Ω
$I_{g(max\ publ.)}$	1·5	2·4	2·4	3·5	A
P_{load}	13·5	25·5	25·8	53·5	kW
p_a	4·15	8·45	7·85	18·4	kW
P_{cct}	1·83	3·5	3·8	5·0	kW
P_{out}	16·25	31·6	32·65	61·6	kW
η_a	79·5	79·0	80·5	77·0	%
η_{load}	66·0	63·0	63·5	67·0	%
η_{trans}	85·0	83·0	82·0	87·0	%
*$P_{grid\ resistor}$	0·414	0·80	0·894	1·32	kW
*p_g	0·303	0·592	0·52	0·74	kW
*P_{drive}	0·717	1·392	1·414	2·06	kW
†$T_{anode\ seal}$	< 149	< 149	< 149	< 149	°C
†$T_{grid\ seal}$	170	149	149	< 170	°C
†$T_{cathode\ seal}$	191	185§	185§	185§	°C
†$T_{filament\ seal}$	< 204	170	170	195§	°C

*Calculated.

†Seal temperature measurements were made without any air cooling.

§Final approximate temperature.

Losses unaccounted for (P_{loss}) include cabinet and radiation losses and these are given by:

$$P_{loss} = P_{out} - P_{load} - P_{cct} - P_{drive}.$$

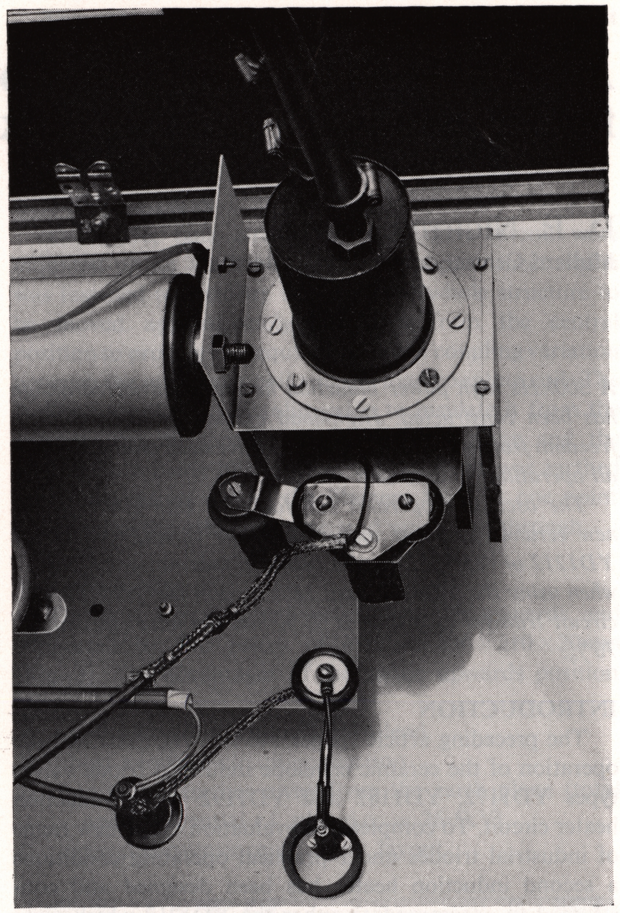

Fig. 7—An overhead rear view of the YD1182 showing particularly some of the grid components

Therefore

	YD1172	YD1182		YD1192
$P_{loss} =$	0·245	1·21	1·64	1·04 kW.

These figures as a percentage of P_{out} are:

1·5	3·8	5·0	1·7	%.

Note: Since the figure for P_{loss} is obtained by subtraction of relatively large measured or calculated powers from the input, small errors in these measurements produce greater errors in the figure obtained for P_{loss}.

Switched overload and off-load switching tests on the oscillator were satisfactory; no parasitic oscillations were evident. The oscillator was overloaded to the point where I_g was reduced to 0·1A and 0·9A for the YD1172 and YD1182 respectively. Power supply limitations prevented an overload test on the YD1192.

With the YD1192 in circuit the grid coil became warm. For a final design a larger diameter tubing (8mm) would alleviate this problem.

Tests were carried out with pieces of mild steel block and tube and the time required to heat such samples to red heat was consistent with the expected load power, having regard to the mass of the individual test pieces.

With the YD1182 in circuit the effect of earthing the load circuit was examined. Each of the points A, B and C in Fig. 1 was earthed in turn to the cabinet by a low inductance copper strap, but no change in operation could be detected.

A 300kHz Induction Heater of Advanced Design for Powers up to 120kW/240kW

D. E. NIGHTINGALE
Mullard Central Application Laboratory

A 300kHz high power induction heater of advanced design has been constructed. High load efficiencies and complete freedom from parasitic oscillations have been obtained under all operating conditions.

The oscillator operates satisfactorily with either of the new ceramic envelope industrial triode valves, namely the YD1212 or YD1202. It will deliver a load power of 226kW when using the YD1212, and 110kW with the YD1202. The circuit transfer efficiency is 95% and the load efficiency is 70%.

INTRODUCTION

The preceding article (pages 146 to 149), described the operation of the ceramic envelope industrial triode valves types YD1172, YD1182 and YD1192 in an induction heater circuit. To complete the evaluation of the new range of industrial triodes under practical operating conditions a second induction heater has been designed and constructed to accommodate either the YD1212 which gives an output power of more than 250kW, or the YD1202 which is rated for half this power. The oscillator (Fig. 1) is a modified form of that described in the above-mentioned article, and is contained in an aluminium cabinet 2m long ×1·5m high ×1·2m deep mounted on an aluminium framework 600mm high (Fig. 2).

The general design principles governing the construction of this generator are equally applicable at other frequencies, at higher loaded Q values, and with other load circuit systems.

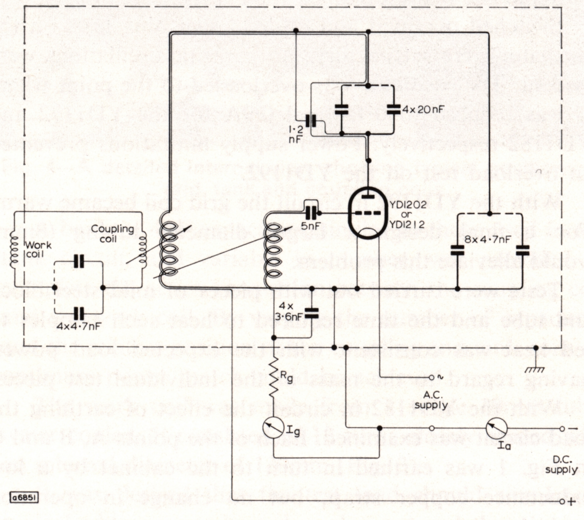

Fig. 1—Circuit of induction heater oscillator

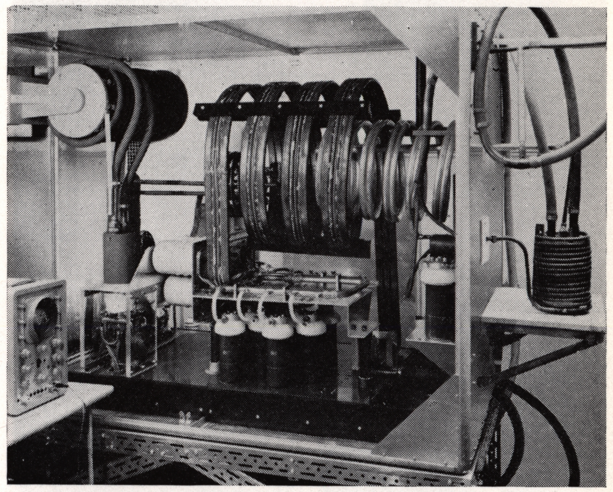

Fig. 2—General view of induction heater

CIRCUIT DESIGN

It was shown in the work on the lower power valves that it is possible to build a generator which is composed of little more than the basic r.f. components without r.f. filtering systems for the valve electrode supplies, provided that the layout of the components is carefully considered. The results obtained proved that stable oscillation could be maintained under all operating conditions without the generation of parasitic oscillations. The absence of spurious oscillations removes the need for parasitic suppression circuits together with the attendant disadvantages such as the creation of further possible parasitic paths and consequent fundamental power losses.

The design for the YD1212 triode is on similar lines to those for the lower power valves but with one basic difference. To cover a range of operating conditions the coupling between the oscillator and the load must be made continuously variable. The load coupling coil and the work coil are partially resonated with a series capacitive reactance to oppose the inductive reactance of the load. The variation of coupling could be achieved by capacitive or inductive changes in the load circuit. Since the available capacitors, by their physical limitations, will only permit changes in discrete steps, and changes in the inductors are fraught with constructional difficulties, a system was adopted to give continuously variable coupling by altering the relative position of the coupling coil and tank coil. The load position was fixed; at the required power level it was undesirable to have flexible leads carrying high r.f. currents as would be required if the coupling coil were moved relative to the load position. Therefore the coupling coil was fixed in relation to the cabinet and work position and the whole of the basic generator was made moveable within the cabinet. This was achieved by mounting the valve, together with its tank circuit and feedback circuit, on an earth plane mounted on an insulated trolley. The earth plane was connected to the earthed cabinet at one point only by a flexible connection. Such a system becomes practicable with valves of a high power/volume ratio, which is a feature of the new range of industrial triodes.

Since the YD1212 has a mutual conductance of 200mA/V it was necessary in the design to ensure that there was no possibility of an unwanted feedback path being provided.

TANK CIRCUIT CALCULATIONS

The following operating conditions are abstracted from the published data on the YD1212:

$f = 300\text{kHz}$
$V_a = 14\text{kV}$
$I_a = 23{\cdot}5\text{A}$
$V_g = -820\text{V}$
I_g (on load) $= 6{\cdot}0\text{A}$
$R_{g-f} = 135\Omega$
$P_{out} = 247{\cdot}5\text{kW}$
$\eta_a = 75{\cdot}2\%$
P_{out} (less P_{drive}) $= 240\text{kW}$
$P_{load} = 215\text{kW}$ at 90% transfer efficiency.

Since one of the design aims of the exercise was to prove the freedom from spurious oscillations at all possible operating conditions a Q value of 25 at full power, 240kW, was chosen.

At full load conditions:

$$V_a = 14\text{kV}$$

and

$$v_{a\ (pk)} = 12{\cdot}5\text{kV}.$$

The r.m.s. value of the peak anode voltage swing is given by:

$$V_{r.m.s.} = v_{a(pk)}/\sqrt{2} = 8{\cdot}85\text{kV}.$$

The loaded $Q(Q_L)$ of the tank circuit is given by:

$$Q_L = \frac{{V_{a(r.m.s.)}}^2}{X_C \times P_{out}}$$

where X_C is the capacitive reactance, so that

$$25 = \frac{8{\cdot}85^2 \times 10^6}{X_C \times 247{\cdot}5 \times 10^3}.$$

Therefore

$$X_C = 12{\cdot}6\Omega.$$

At 300kHz $C = 42\text{nF}$ and the total tank circulating current is given by:

$$V_{r.m.s.}/X_C = 8{\cdot}85 \times 10^3/12{\cdot}6 = 702\text{A}.$$

A suitable capacitor can be built up from eight water cooled ceramic capacitors, Mullard type TW85/260, 4·7nF rated at 14kV, 140A. A safety margin on the current rating is required to permit no-load operation (giving an increased tank circuit voltage swing).

The actual value of the tank circuit capacitance used was therefore:

$$8 \times 4{\cdot}7\text{nF} = 37{\cdot}6\text{nF}.$$

This value gives a reactance of 14·1Ω. The loaded Q at full power is now given by:

$$Q_L = \frac{8{\cdot}85^2 \times 10^6}{14{\cdot}1 \times 247{\cdot}5 \times 10^3} = 22.$$

Since $X_C = X_L$, then $X_L = 14{\cdot}1\Omega$, and $L = 7{\cdot}5\mu\text{H}$.

CONSTRUCTION

The valve, tank circuit and grid drive circuit were mounted on an earth plane of 2mm copper sheet which was fastened to a trolley to enable the whole structure to be moved approximately ±200mm from the central position to provide the required degree of coupling variation between the main tank coil and the load coupling coil. The trolley runs along a Paxolin guide to insulate it from the cabinet; the distance between the earth plane and the cabinet floor being 100mm (Fig. 2). The plane was earthed to the chassis by one of the filament leads at one point only, where the other filament lead was taken through.

Valve Mounting

The valve was mounted vertically, anode upwards, and supported by two pieces of Perspex 330×210×20mm (Fig. 3). The advantages of the anode upwards position were:

1) short cathode-to-circuit return lead
2) short anode-to-circuit connection
3) anode was further away from the earth plane (total anode potential r.f. plus d.c. = 26·5kV)
4) general convenience of circuit layout.

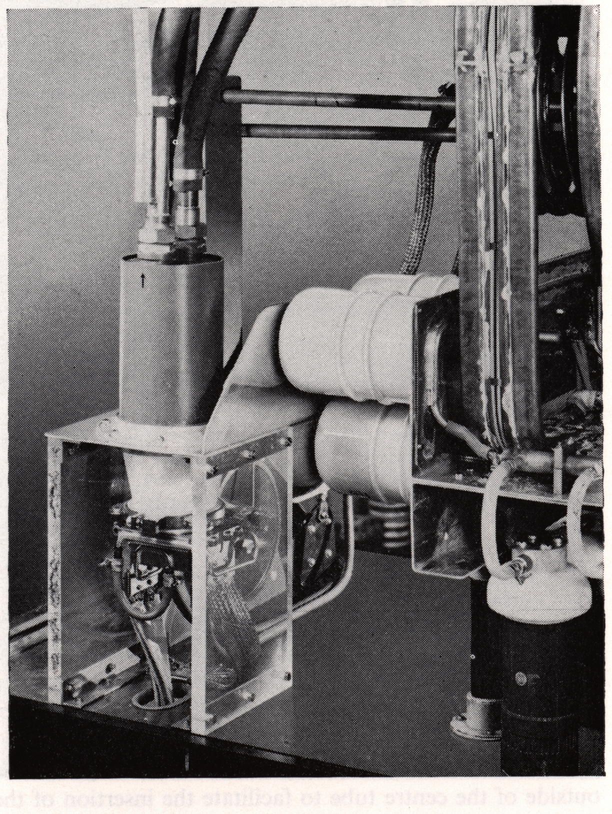

Fig. 3—The YD1212 is shown mounted on Perspex side panels. The thermometer with which the rise in temperature of the anode cooling water is read can be seen attached to one of the water feed pipes

The disadvantage was the problem which arose when changing valves especially if a valve with a separate water jacket was used. Simple taps mounted in the water supply at the anode end of the anode hose coil overcame this minor problem.

Tank Capacitor

The tank capacitance consisted of a block of eight water-cooled ceramic capacitors, Mullard type TW85/260, connected in parallel. The capacitors were rigidly mounted on the 2mm copper earth plane by the base mounting screws. The upper (live) terminals were connected by short low inductance flexible copper straps to a large area aluminium plate which was mounted on three glass insulating pillars to provide the main support for the live end of the tank coil and the anode blocking capacitors (Figs. 2 and 4).

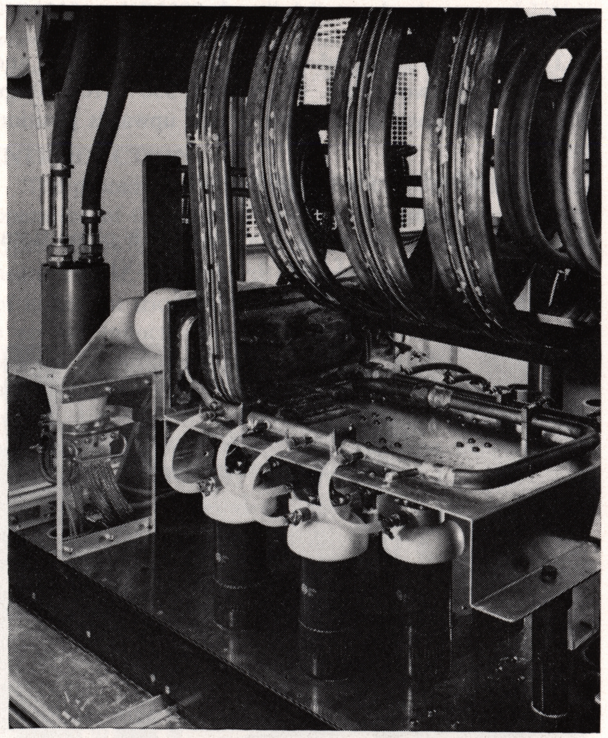

Fig. 4—General view of the tank circuit showing the water cooling arrangements. The water manifold system for the tank capacitors, and the cooling system of the plate which supports the anode blocking capacitors, can be seen in the centre

Tank Coil

The tank inductor, of 3½ turns, was formed from three 28mm diameter copper tubes slightly flattened and brazed together side by side to give a total width of a composite turn of 100mm. The internal diameter of the coil was 650mm and the length was 600mm.

A 10mm wide slot was cut down the full length of the outside of the centre tube to facilitate the insertion of the three parallel connected high voltage cables carrying the anode d.c. supply. Such an h.t. feed system eliminated the need for a separate anode choke. The respective r.f. low and high potential ends of the coil can be seen in Figs. 5 and 6. The r.f. high potential ends of the inductor were connected to a manifold system which distributed the cooling water flowing through the two outer tubes to and from the ceramic tank capacitors; their water connections were also at the same high r.f. potential. The cooling water entered and left the coil at its earthy end and needed no further decoupling. Since part of the common connecting plate from the tank circuit to the blocking capacitors was in the field of the tank coil a small water flow in parallel with the tank capacitors had to be diverted for the purpose of contact cooling the upright part of the plate (Fig. 6).

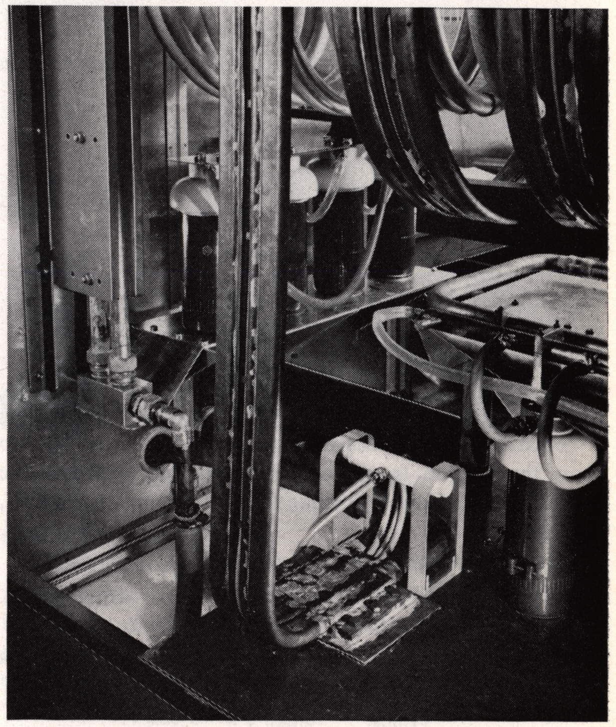

Fig. 5—H.T. input connection to the tank circuit can be seen in the foreground, with part of the load coupling circuit above it

Grid Coil

The aperiodic grid coil consisted of 4 turns of 15mm copper tubing. The coil was 260mm in diameter spaced to give a total active length of 150mm. An 8mm copper pipe was soldered on the outside of the coil to carry a small flow of cooling water. This was necessary as the coil was heated by eddy currents through being in the r.f. field of the tank coil. To eliminate the need for a separate grid choke the lead carrying the d.c. grid current formed an inner conductor to the grid coil. The ends of the coil were terminated in a length of braided copper sleeving to allow for positional adjustment of the coil. The water connections to the coil were taken through rubber hose pipes through the braid together with the wire for the d.c. grid connection. The coil was mounted on a simple slide to permit variation of drive by altering the position of the grid coil with respect to the main tank coil (Figs. 7 and 8).

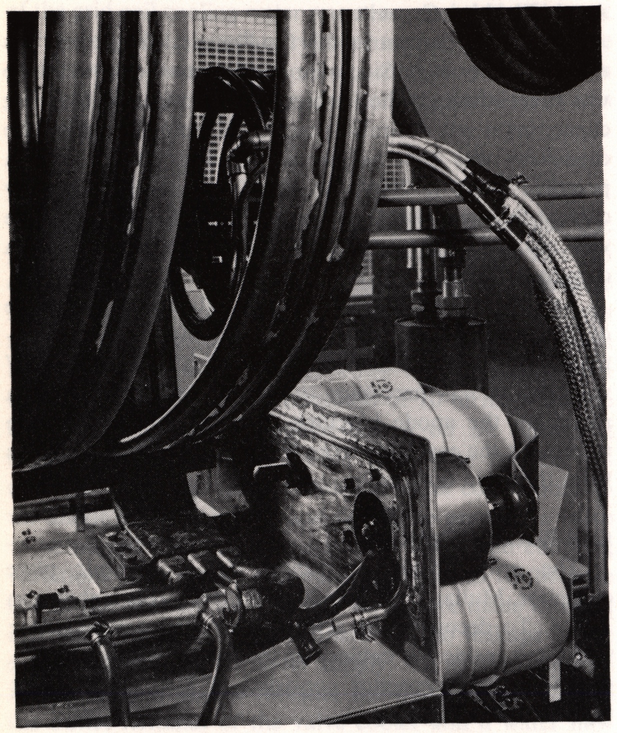

Fig. 6—D.C. and r.f. feed arrangements to the valve are shown in the foreground. Water cooling of the grid coil is carried out by the pipes shown right and centre, above the blocking capacitors and valve

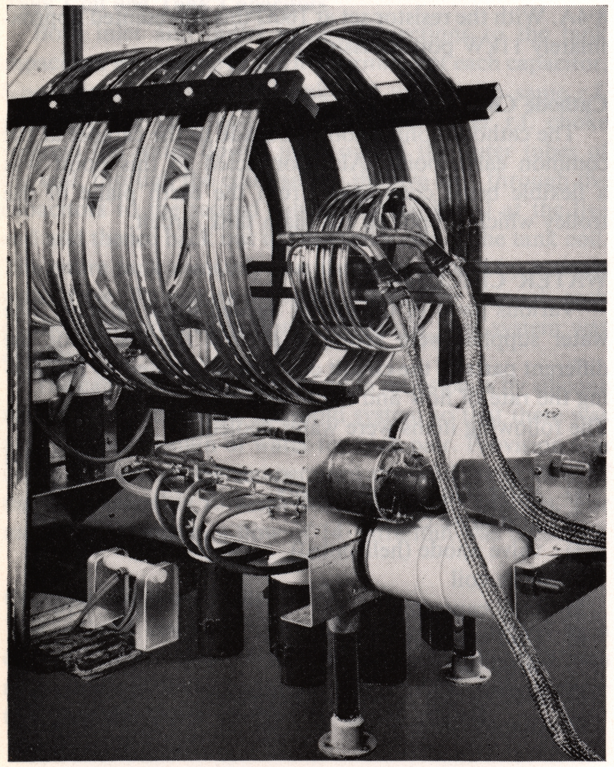

Fig. 7—General view of the oscillator circuit, showing the tank coil, and the grid coil with its flexible braid connections

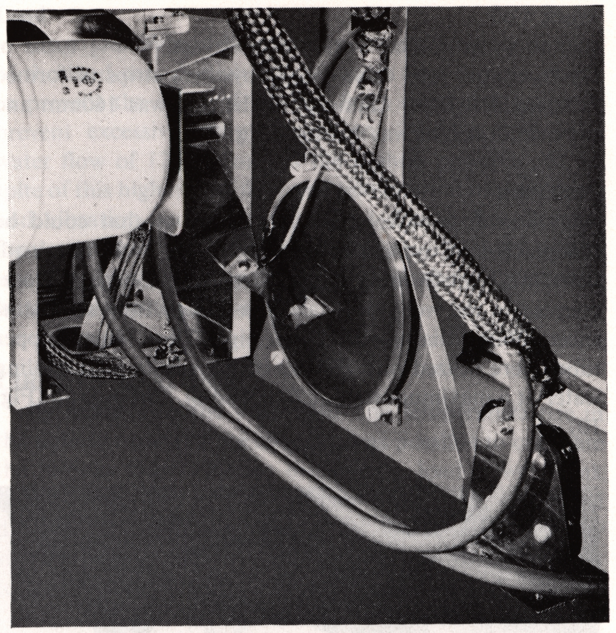

Fig. 8—Grid blocking capacitor

Load Coupling Coil

The water cooled load coupling coil consisted of two 28mm tubes spot brazed in parallel. To give adequate load coupling range there were 6 turns of 400mm overall diameter, occupying a length of 600mm (Fig. 9).

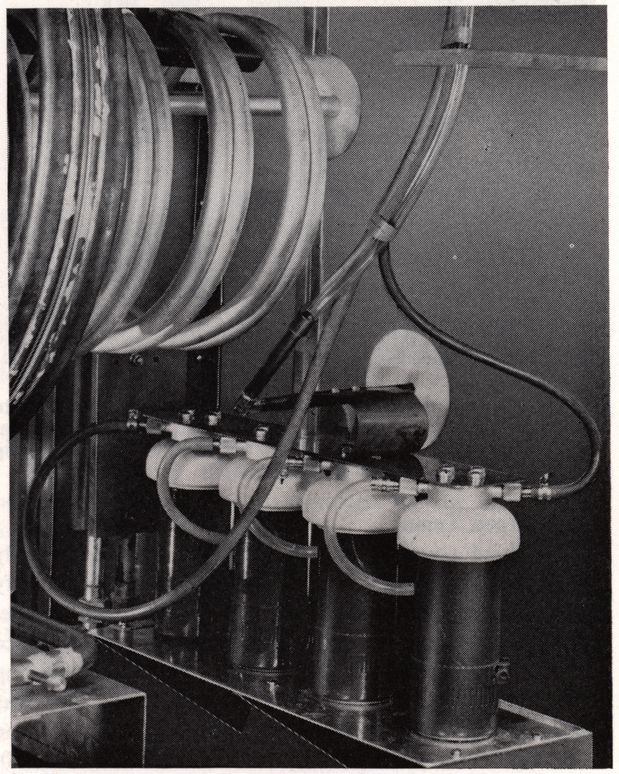

Fig. 9—Coupling circuit capacitors. The three interconnecting water hoses shown between the capacitors are dressed to lie over the top connecting plate and not as shown. This avoids flash-over problems

Work Coil

The water cooled work coil consisted of 14½ turns of 16mm copper tube close spaced by three strips of formed Paxolin. The inner diameter of the coil was 160mm and the overall height was 250mm (Fig. 10).

Test Load

It was decided to measure the power that could be dissipated in a typical induction heated load. The load, therefore, consisted of a water cooled steel can, close-coupled to the work coil, fabricated from 1mm mild steel sheet 150mm diameter, 200mm high. Two 28mm copper tubes were brazed into the top of the can to pass cooling water at a maximum rate at full load of 120litre/min (Fig. 10).

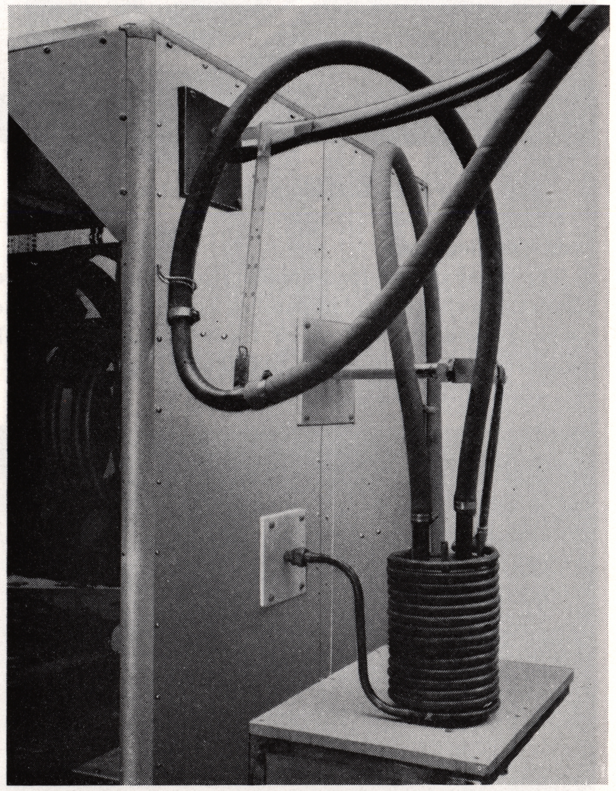

Fig. 10—Work coil with load can inside and thermometer to indicate the temperature rise of the cooling water. The framework of the mounting table shown is slotted to avoid coupling to the work coil

Load Circuit Tuning

The load coupling coil and work coil were partially series resonated, as is carried out in practice, to simplify load coupling problems. With the steel can load close-coupled to the work coil described, the capacitance required to near-resonate the entire load circuit including both load coupling and work coils was 19nF. This was obtained conveniently by using four capacitors of the same type as the main tank capacitors, Mullard TW85/260, 4·7nF, 140A. The capacitors were parallel connected in such a way that more or fewer units could be connected in circuit to accommodate other loads and load coil dimensions.

Anode Blocking Capacitor

The anode current at the fundamental frequency was approximately 40A. Since the d.c. feed to the valve anode was taken through the tank coil and across the blocking capacitors it was desirable that the r.f. potential across the capacitors was kept as low as possible. At full load a practical figure is 260V. At 40A fundamental frequency current this required a reactance of 6·7Ω. Such a reactance was obtained conveniently by using four 20nF mica capacitors T.C.C. type 1053.

As an added safeguard the d.c. feed line from the inside of the tank coil was decoupled by a high voltage feed-through capacitor, Mullard DW45/150 K90, 1·2nF, 16kV working. It was necessary to mount the capacitor in a recess on the anode blocking capacitor mounting plate to prevent the capacitor from being heated by r.f. currents from the main tank coil.

Grid Blocking Capacitor

The grid blocking capacitor was a ceramic plate capacitor, Mullard type FPa200 K90, 5nF. This is shown in Fig. 8. To decouple the grid resistor a bypass capacitor was fitted inside the cabinet to the earthy end of the d.c. grid feed. The capacitor consisted of 4 x 3·6nF, Hunt type CZ5387 (Fig. 8).

Grid Resistor

The grid resistor was constructed of a number of series/parallel connected resistance 'mats' in a frame to permit cooling by an air blast. The maximum dissipation occurred in an off-load condition where the grid current rose to 8·4A. With the resistor set at 160Ω this represented approximately 11kW power dissipation.

Cathode Connection

The cathode connection was made to the cabinet at the common earth point. Also connected to this point was a flexible braid connection from the earth plane of the trolley which supported the main tank circuit.

WATER CIRCUITS

Various parts of the circuit needed water cooling. The water supplies were arranged so that the losses for the different parts of the circuit could be calculated by measuring the rate of flow and the temperature rise.
The following items were water cooled:

		litre/min
1)	valve filament connectors	0·5
2)	grid drive coil	0·5
3)	valve anode (helicooled)	60
4)	tank coil	14·3
5)	tank capacitors	14·3
6)	load coupling coil	6·2
7)	work coil	6·2
8)	load circuit resonating capacitors	1·0
9)	dummy load	120

Filament Connectors and Grid Coil

The filament connectors and grid coil shared a common water flow, the grid coil cooling water being arranged in series with that for the filament connectors. The live end of the grid coil cooling water was connected to the filament water circuit by a length of rubber hose sufficient to ensure minimum r.f. losses in the cooling water. No provision was made to measure the power loss in this water since it was insignificant.

Anode

Since the anode operated at 26·5kV peak r.f. plus d.c. potential it was necessary to feed the valve anode through columns of water sufficiently long to prevent noticeable loss of power due to heating of the water by r.f. currents and d.c. To prevent radiation losses from the water hose both input and output water flows were arranged as a bifilar water choke which consisted of 10 turns of double hose (inlet and outlet) space-wound on an insulating former 250mm diameter 1·05m long. The former was mounted inside the cabinet with the water connections to the anode sufficiently long and flexible to permit the valve to be moved with the tank assembly when load coupling variations were made. The water connections to the hose coil at the end remote from the valve were made through earthed pipes to ensure that there was no leakage of r.f. currents or d.c. to the water supply. An alcohol thermometer was arranged to measure the water temperature at the outlet terminal of the valve cooler and a water flow meter was included in this water circuit to permit measurements of total valve dissipation to be made. (For most of the measurements on the YD1212 a water flow of 60litre/min was used.)

Tank Coil and Tank Capacitors

Both inlet and outlet water connections to the tank capacitors were made to the live terminal of each capacitor. Since the live end of the tank coil was at the same r.f. potential, the tank coil was used as a water r.f. choke wherein the water flowed in to one of the outer tubes of the coil, through the coil itself to the live end, through the capacitors to the second tube of the tank coil at the live end and thence back out to the earthy end of the tank coil. The entire tank assembly was therefore cooled by a single water flow. To ensure a similar water flow through each of the eight tank capacitors a manifold pipe system was employed.

The capacitors were connected in series pairs by silicone rubber pipes across the manifold system so that there was a similar path length of water for each pair. Provision was made to monitor the temperature rise and water flow of the tank assembly to assist with the circuit analysis. For most measurements a flow of 14·3litre/min was used.

Coupling and Work Coils

The load coupling and work coils were cooled by a common water flow of 6·2litre/min, and provision was made to monitor the temperature rise of the cooling water to assess the losses in this part of the circuit.

Load Circuit Resonating Capacitor

The load circuit capacitors were cooled by a water flow of about 1·0litre/min. This was not monitored as the temperature rise was small and the power loss insignificant.

Load

Up to 240kW was dissipated in the relatively small mass of the load can. A high rate of water flow was necessary to prevent the walls of the can from overheating and to prevent excessive steam formation. This resulted in a water flow of 120litre/min at the highest power input. In spite of this high rate of flow a certain amount of simmering and vibration occurred in the load due to the alternate formation and condensation of steam. The load power was calculated by noting the temperature rise of the cooling water at the water flow used.

CIRCUIT ANALYSIS

By monitoring the water flow and temperature rise in the different parts of the circuit it was possible to calculate the various losses. Anode dissipation, load power, tank circuit losses and coupling circuit losses were calculated directly and the remainder of the losses was found by subtracting the calculated losses from the total d.c. input to the generator.

Input Power

The total d.c. input power to the generator was divided into the following parts which were found either by calculation or subtraction:

Anode dissipation	(p_a)
Load power	(P_{load})
Tank circuit losses	
Coupling circuit losses	
Grid dissipation	(p_g)
Bias loss	(P_B)
Cabinet and radiation losses	

Output Power

The total valve output power was found by subtracting the calculated anode dissipation from the input power

$$P_{out} = P_{in} - p_a. \qquad \ldots(1)$$

Load Power

The load power was calculated directly from the water flow and the temperature rise of the load cooling water.

Drive Power and Circuit Losses

By subtracting the calculated load power from the output power a figure was obtained for the total circuit losses including drive power

$$P_{out} - P_{load} = P_{circuit(total)} + P_{drive}. \qquad \ldots(2)$$

Grid Dissipation

The grid dissipation was calculated from the approximate relation:

$$p_g = 0{\cdot}9 \times I_g \times v_{g(pk)}. \qquad \ldots(3)$$

Bias Loss

The bias loss was calculated from the product of the grid resistor and the square of the grid current

$$P_B = R_g \times I_g^2. \qquad \ldots(4)$$

TABLE 1

Results Obtained for Various Input and Output Powers

YD1212

V_a (kV)	I_a (A)	P_{in} (kW)	I_g (A)	p_g (kW)	p_a (kW)	P_{out} (kW)	η_a (%)	P_{load} (kW)	η_{load} (%)	$P_{tank\ cct.}$ (kW)	$P_{load\ cct.}$ (kW)	$\eta_{cct.}$ (%)	R_g (Ω)	P_{drive} (kW)
10·0	22·0	220	5·65	2·2	56	164	74·4	150	69·2	3·1	6·6	95·5	130	6·35
11·0	14·75	162	4·1	1·1	38	124	76·4	113	69·9	4·5	4·2	94·5	160	3·79
12·0	13·9	167	3·9	1·0	42	125	75·0	115	69·0	5·9	6·7	94·5	160	3·44
12·0	3·0	36	7·1	2·0			Off load						160	
12·0	18·8	226	4·45	1·5	55	171	75·7	155	68·7	4·5	6·7	93·0	160	4·67
12·0	3·1	37	7·5	2·1			Off load						160	
12·0	25·2	303	5·0	2·0	88	215	71·0	201	66·4	4·0	8·3	96·0	140	5·5*
13·0	9·8	127	3·65	0·8	31	96	75·5	80	63·0	7·5	5·0	86·5	160	2·93
13·0	3·2	42	7·7	2·1			Off load						160	
13·0	17·0	221	4·9	1·5	52	169	76·6	155	70·1	6·6	6·0	95·0	160	5·35
13·0	23·1	300	5·7	2·3	71	229	76·3	213	71·0	5·7	9·7	96·5	160	7·5
14·0	16·2	227	4·25	1·2	56	171	75·4	156	68·3	6·8	6·5	93·5	160	4·1
14·0	3·0	42	6·6	1·9			Off load						160	–
14·0	21·3	298	4·1	1·3	78	220	74·0	202	67·8	5·9	8·5	94·0	160	4·0
14·0	3·3	46	7·2	2·0			Off load						160	–
14·0	21·2	297	4·4	1·4	75	222	75·0	205	69·0	6·2	8·6	94·5	160	4·5
14·0	3·2	45	7·4	2·1			Off load						160	–
14·0	23·6	330	6·15	2·7	75	255	77·3	228	69·1	6·8	10·2	93·0	160	8·75¶
14·0	23·6	330	4·2	1·4	94	236	71·5	222	67·5	5·8	10·0	95·5	160	4·22§
14·0	3·6	50	7·9	2·2			Off load						160	–
14·0	23·8	334	4·7	1·5	86	248	74·2	228	68·4	5·5	9·4	94·0	160	5·03‖
14·0	3·5	49	8·4	2·3			Off load						160	–
14·0	23·5	329	4·5	1·4	88	241	73·2	226	68·8	5·7	10·7	95·5	160	4·65†
							YD1202							
10·0	15·8	158	3·5	1·8	33	125	79·2	111	70·6	3·2	4·5	92·5	200	4·25
12·0	13·0	156	2·7	1·2	31	125	80·0	110	70·6	5·0	4·5	91·0	300	3·38

* Reduced R_g † -10% V_f § Low drive ‖ Medium drive ¶ High drive

Drive Power

If the very small grid circuit loss was ignored the drive power was made up of the bias loss and the grid dissipation

$$P_{drive} = P_B + p_g. \quad \ldots(5)$$

Circuit Losses

By subtracting the drive power and the load power from the output power a figure was obtained for the total circuit losses

$$P_{circuit(total)} = P_{out} - P_{drive} - P_{load}. \quad \ldots(6)$$

Radiation and Cabinet Losses

The power loss in the tank circuit and coupling coil was calculated from the temperature rise of the cooling water in these components and when this figure was subtracted from the total circuit loss (as found in the previous paragraph) a figure for radiation losses and cabinet losses was obtained.

RESULTS

The complete results obtained are given in Table 1. For the recorded off-load condition the load circuit was opened, thus representing a complete electrical removal of any coupling to the tank circuit. This condition would not normally arise in practice, and practical off-load grid currents are likely to be lower. Results obtained with the YD1202 are also shown.

The waveform was satisfactory, being a sinewave with a superimposed ripple of about the 20th harmonic at less than 10% of the fundamental amplitude. There were no sharp spikes or other evidence of instability at any operating condition, loaded or unloaded.

ACKNOWLEDGEMENT

The invaluable assistance of the staff of the Philips' High Power Measurements Laboratory, and the active co-operation of the workshop staff of the Philips' Transmitting Valve Development Laboratory, contributed greatly to the success of this project.